May 2017

Electrophysiological and Morphological Characterization of Neurons in the Granular Retrosplenial Cortex

Andrew Nicholas Nye
University of Wisconsin-Milwaukee

ELECTROPHYSIOLOGICAL AND MORPHOLOGICAL CHARACTERIZATION OF NEURONS IN THE GRANULAR RETROSPLENIAL CORTEX

by

Andrew Nye

A Thesis Submitted in

Partial Fulfillment of the

Requirements for the Degree of

Master of Science

in Psychology

at

The University of Wisconsin-Milwaukee

May 2017

ABSTRACT

ELECTROPHYSIOLOGICAL AND MORPHOLOGICAL CHARACTERIZATION OF NEURONS IN THE GRANULAR RETROSPLENIAL CORTEX

by

Andrew Nye

The University of Wisconsin Milwaukee, 2017
Under the Supervision of Professor James R. Moyer Jr.

The retrosplenial cortex (RSC) is a centrally located brain region that has reciprocal connections with several brain regions important for memory, including the prefrontal cortex, para-hippocampal region, hippocampal formation, and rhinal cortices. The RSC is also well connected with structures important for sensory processing, including the parietal cortex, thalamus, and visual cortices. Due to this connectivity, and early evidence that suggests the RSC plays a critical role in learning and memory, the region has recently gained much more research attention. Early studies found that patients with brain damage that includes the RSC have difficulty with verbal and visual information, retrieving recent autobiographical memories, and spatial navigation. Likewise, human research with neurologically intact participants suggests that the RSC could be involved in a wide range of cognitive processes, and early animal research supports this hypothesis as well. Specifically, rodent research on the RSC has demonstrated that the region supports tasks that involve spatial navigation, fear memory, and object recognition. For spatial tasks, the RSC seems to specifically be important for the use of distal cues to complete tasks like the radial arm maze, T-maze, and Morris water maze. For fear memory, the RSC is important for both trace and context fear memory, as well as extinguishing conditioned fear memory. Due to these findings, the RSC should be aggressively researched so that a complete understanding of the region and potential treatments for memory disorders and PTSD

may be achieved in the near future. A large gap in our knowledge of the RSC is how the structure functions on the cellular level. *In vivo* electrophysiological studies, found that the RSC contains direction cells, and is active during the encoding of navigational cues, the encoding of a reward and its location, and during goal directed navigation. One study has examined the RSC at the single cell level, and reported regular-spiking and late-spiking neurons, but did not thoroughly characterize neurons in the RSC. Thus, the intrinsic electrophysiological and morphological properties of neurons in the RSC have not been thoroughly characterized. The present study sought to fill this gap in our knowledge of the RSC, and found four distinct populations of cells. Characterized by their firing patterns, neurons were classified as regular-spiking with a pronounced afterdepolarization (ADP-RS), double-spiking (DS), fast-spiking (FS), and late-spiking (LS) neurons. The current study examined intrinsic electrophysiological and morphological properties of these neurons and the underlying mechanisms mediating the afterdepolarization (ADP) and fast-spiking (FS) properties observed in granular retrosplenial cortical neurons. Using the synaptic blockers CNQX and D-AP5, we found that ionotropic glutamatergic synaptic input doesn't significantly impact either of these properties. Using group 1 metabotropic glutamate receptor blockers LY367385 and MPEP we determined that the ADP property is at least partially mediated by these receptors. We used TEA to determine if the FS property is mediated by the voltage gated K^+ channels Kv3.1-Kv3.2, and found that the FS property is likely partially mediated by these channels. These findings provide a foundation for understanding how the RSC may function to perform its important functions as well as shed light on how it may interact with other interconnected brain regions.

TABLE OF CONTENTS

LIST OF FIGURES

LIST OF TABLES

ACKNOWLEDGEMENTS

I would like to thank my advisor Dr. James R. Moyer Jr. for his guidance and help throughout this project. I would also like to thank my committee members, Dr. Fred Helmstetter and Dr. Kamran Diba for their advice and feedback on my thesis. Thanks to Jenna Tuma for her assistance with neuronal reconstructions. I want to extend my gratitude to Vanessa Ehlers, Shane Pullins, and Hanna Yousuf for their advice and support throughout this project.

Introduction

The current understanding of memory involves multiple regions of the brain working together to both encode and retrieve memories. The hippocampus is critical for both memory encoding (McEchron et al., 1998; McEchron et al., 2000; Misane et al., 2005; Moyer, Deyo, & Disterhoft, 1990) and memory retrieval (Fabbri et al., 2016; Tanaka et al., 2014). The medial prefrontal cortex (mPFC) is similarly important for both memory encoding (Gilmartin & Helmstetter, 2010; Vidal-Gonzalez, Vidal-Gonzalez, Rauch, & Quirk, 2006) and memory retrieval (Runyan, Moore, & Dash, 2004), as well as modifying memories to incorporate new information (Burgos-Robles, Vidal-Gonzalez, Santini, & Quirk, 2007; Burgos-Robles, Vidal-Gonzalez, & Quirk, 2009; Chang & Maren, 2011; Vidal-Gonzalez et al., 2006). Additionally, the amygdala is vital for both the encoding (Helmstetter, 1992; Helmstetter & Bellgowan, 1994; Maren, Aharonov, & Fanselow, 1996) and the retrieval (Anglada-Figueroa & Quirk, 2005; Gale et al., 2004; Kwapis, Jarome, Schiff, & Helmstetter, 2011; Maren et al., 1996) of fear memories. Although, the details of the relationships between these brain regions and other brain regions associated with memory are still being investigated. For example, the retrosplenial cortex (RSC) is a region of the brain that is centrally located near regions important for memory, and early evidence that suggests it plays a critical role in learning and memory. This evidence comes from patients with brain damage that includes the RSC who consequently have difficulty with verbal and visual information, retrieving recent autobiographical memories, and spatial navigation (see review Vann, Aggleton, & Maguire, 2009). However, since brain injuries are rarely precise enough to draw strong conclusions from the deficits observed in patients, these cases raised questions about the precise function of the RSC. Research using animal models has begun to answer these questions and will be discussed in subsequent sections.

The quest to fully understand the RSC is also driven by the need to treat humans with aging-related cognitive decline (Andrews-Hanna et al., 2007; Bishop, Lu, & Yanker, 2010). Approximately 85 million or 22% of the United States population will be over 65 by 2050 (Ortman, Velkoff, & Hogan, 2014), and this large population of people are currently facing or will face serious public health issues, such as aging-related cognitive decline and Alzheimer's disease. In the United States, the prevalence of Alzheimer's disease in people 65 and older is 10%, and by age 85 and older this rate jumps to 32% (Alzheimer's Association, 2017). In rodents, aging-related changes in memory function have been well characterized in both the hippocampus and the mPFC. For example, trace and contextual fear memory rely on the hippocampus and the mPFC (Gilmartin & Helmstetter, 2010; McEchron, Bouwmeester, Tseng, Weiss, & Disterhoft 1998; McEchron, Tseng, & Disterhoft, 2000; Runyan et al., 2004), and aging-related deficits in these types of memory are well documented (McEchron, Cheng, & Gilmartin, 2004; Moyer & Brown, 2006; Villarreal, Dykes, & Barea-Rodriguez, 2004). Furthermore, aging-related changes in electrophysiological function within the hippocampus and mPFC are coupled with aging-related deficits in context fear memory and extinction of conditioned fear memory (Kaczorowski & Disterhoft, 2009; Kaczorowski, Davis, & Moyer, 2012).

Although normal aging-related physiological dysfunction of the RSC has not been investigated, human research has found that the RSC is among the first brain regions to display atrophy and a decline in metabolic function in Alzheimer's patients (Pengas, Hodges, Watson, & Nestor, 2010; Villain et al., 2008), and thus may contribute to early symptoms of Alzheimer's disease. Due to these findings, the RSC should be aggressively researched so that a complete understanding of the region may be achieved in the near future, because the ability to

characterize and understand aging-related changes in memory function will always be limited by the understanding of normal memory function. Obtaining a comprehensive understanding of the RSC is critical to develop interventions and treatments for aberrant changes in memory that occur with normal and non-normal aging.

Anatomy and Connectivity of the RSC

There are several reasons for piqued interest in the RSC, primarily because its location poses potentially significant connections and functions. The human RSC is located just posterior of the hippocampal formation and just anterior of the occipital cortex (Vann et al., 2009). Likewise, the rat RSC is located dorsal of the hippocampus and hippocampal formation, and anterodorsally to sensory cortices (Paxinos & Watson, 2007). The central location and large size of the RSC in both humans and rats suggests that it may play a role in memory and integrating sensory information into memories. This would be accomplished by having an abundance of reciprocating connections with neighboring brain regions including the hippocampus and sensory cortices. Although the details of functional RSC connections are still being investigated, it is clear that the RSC is highly connected with itself and neighboring brain regions including the prefrontal cortex, cingulate cortex, temporal lobe, para-hippocampal region, hippocampal formation, parietal cortex, thalamus, rhinal cortices, and visual cortices (Aggleton, Wright, Vann, & Saunders, 2012; Aggleton, Saunders, Wright & Vann, 2014; Burwell & Amaral, 1998; Czajkowski et al., 2013; Kobayashi & Amaral, 2003, 2007; Miyashita & Rockland, 2007; Morris, Pandya, & Petrides, 1999; Oda et al., 2014; Prasad & Chudasama, 2013; Seltzer & Pandya, 2009; Shibata, Kondo, & Naito, 2004; Shibata & Naito, 2008: Shibata, Honda, Sasaki & Naito, 2009; Sugar, Witter, van Strien, & Cappaert, 2011; van Groen & Wyss, 1990, 1992, 2003; Vann et al., 2009; Vogt & Miller, 1983; Wilber et al., 2015). Notably, the RSC receives

projections from CA1, presubiculum, parasubiculum, and subiculum. Collectively these studies demonstrate that the RSC is well-connected to regions that are important for memory, such as the PFC and hippocampus, which is why it's a region of the brain that deserves research attention.

Interestingly, projections to and from the rat RSC display specific topographical organization based on the layer, sub-region, and anteroposterior location (see review Sugar et al., 2011). For example, the anterior portion of sub-region c of the granular retrosplenial cortex (GRS) projects to the dorsal and middle portion of the subiculum, whereas the posterior portion of sub-region c of the GRS projects to the middle and ventral portion of the subiculum. Reciprocal projections from the subiculum to the RSC display a similar topographical organization (Sugar et al., 2011). Likewise, projections from the septal portion of CA1 terminate in the anterior portion of the GRS sub-region ab. Also, the distal portion of septal CA1 projects to the GRS sub-region c.

The topographical organization of connections that the RSC has with other brain regions appears to be important for the way it processes information. For example, lesioning the anterior thalamic nuclei (ATN) can negatively impact the ability of the RSC to function normally, by reducing RSC spine density (Harland, Collings, McNaughton, Abraham & Dalrymple-Alford, 2014) and reducing RSC immediate early gene expression (Jenkins, Vann, Amin & Aggleton, 2004). Interestingly, both of these effects are specific to layer II/III of the GRS (Harland et al., 2014; Jenkins et al., 2004). This demonstrates the importance of maintaining specificity when studying the RSC, which is why the present study focuses on just the GRS.

Function of the RSC

Even though details of RSC function are still being investigated, many studies have demonstrated that the RSC supports a variety of tasks that involve spatial navigation, fear

memory, object recognition, and autobiographical memory. For example, the RSC is important for the use of distal cues in several spatial navigation tasks, including the radial arm maze, T-maze, and Morris water maze (Cain, Humpartzoomian, & Boon, 2006; Cooper & Mizumori, 2001; Keene & Bucci, 2009; Pothuizen, Davies, Aggleton, & Vann, 2010; Vann & Aggleton, 2005). In regards to fear memory, early studies concluded that the RSC is only involved in the acquisition and retrieval of context fear memory (Corcoran et al., 2011; Keene & Bucci, 2008a; Keene & Bucci, 2008b; Keene & Bucci, 2008c; Robinson, Poorman, Marder, & Bucci, 2012; Sigwald et al., 2015). However, more recent studies demonstrate that the RSC is also important for the acquisition and retrieval of both trace and context fear memory (Kwapis et al., 2015), as well as extinguishing conditioned fear memory (Kwapis, Jarome, Lee, Gilmartin, & Helmstetter, 2014). Recent studies have also determined that the rat RSC is important for object recognition (Haijima & Ichitani, 2012; Hindley, Nelson, Aggleton, & Vann, 2014) and that the human RSC is active during autobiographical memory retrieval (Foster, Kaveh, Dastjerdi, Miller, & Parvizi, 2013).

However, despite the growing body of evidence that associates the RSC with several types of memory, the precise role(s) that the RSC has within memory circuitry is only beginning to be understood. A particularly large gap in the current understanding of the RSC is the underlying physiology of the region. Although a study using immediate-early gene expression verified that the RSC shows increased neuronal activity during fear conditioning (Robinson et al., 2012), little is known about the electrophysiology of the RSC. This current study sought to characterize the intrinsic electrophysiological and morphological properties of neurons within the GRS. Only a few studies have examined functional differences between the GRS and the dysgranular retrosplenial cortex (Hindley et al., 2014; Pothuizen et al., 2010; Vann & Aggleton,

2005), and found minimal differences. However, due to the previously discussed differences in connectivity between the two RSC sub-regions (see review Sugar et al., 2011) the distinction between sub-regions may prove to be important, which is why the current study focused on the GRS.

Intrinsic Excitability

Intrinsic excitability is modulated by electrophysiological properties that determine the likelihood that a neuron will fire an action potential in response to a stimulus. This results in controlled informational throughput of the cell, also called intrinsic plasticity (see reviews Daoudal & Debanne, 2003; Frick & Johnston, 2004; Sehgal, Song, Ehlers, & Moyer, 2013; Zhang & Linden, 2003). The electrophysiological properties that modulate intrinsic excitability include input resistance, afterhyperpolarization (AHP), spike frequency adaptation, resting membrane potential, and multiple action potential (AP) properties, such as AP threshold, AP amplitude, and AP width; and these properties are modulated by the number and activation of various ion channels (Daoudal & Debanne, 2003; Sehgal, Song, Ehlers, & Moyer, 2013; Zhang & Linden, 2003). Furthermore, learning-associated changes in electrophysiological properties that lead to modifications in intrinsic excitability are observed across multiple tasks and multiple brain regions (see table 1). This demonstrates that intrinsic plasticity is a widespread and robust phenomenon that is related to learning and memory.

Strong evidence for the direct relationship between intrinsic plasticity and learning and memory comes from a study that used olfactory discrimination and the Morris Water Maze (MWM), two tasks that are known to increase intrinsic excitability (Oh et al., 2003; Saar et al., 1998). Rats that were first trained on an olfactory discrimination task subsequently displayed enhanced acquisition of the MWM, which was dependent on the olfactory discrimination-

induced increase of intrinsic excitability (Zelcer et al., 2006). However, even stronger evidence comes from a study that demonstrated a gain of function and loss of function through manipulation of intrinsic excitability (Santini & Porter, 2010). First, neuronal intrinsic excitability was assessed after bath applying an M-type K^+ channel antagonist or agonist (XE-991 and flupirtine respectively). XE-991 increased neuronal intrinsic excitability while flupirtine decreased neuronal excitability when bath applied onto slices containing the infralimbic prefrontal cortex. Then an infusion of XE-991 into the infralimbic prefrontal cortex enhanced acquisition and retrieval of extinction learning. In contrast, infusion of flupirtine into the infralimbic prefrontal cortex impaired acquisition and retrieval of extinction learning (Santini & Porter, 2010). Collectively these studies demonstrate that intrinsic excitability plays a critical role in learning and memory and deserves further investigation. It is particularly important to study intrinsic excitability in all brain regions that are thought to be involved in memory processes given the fact that different brain regions can play complementary roles to each other. Examples include the infralimbic (IL) and prelimbic (PL) prefrontal cortices. Recent evidence suggests that the IL is involved in the formation of long term conditioned fear memory, and that the PL plays the complementary role of suppressing conditioned fear (Song et al., 2015). The RSC may serve complementary roles to the hippocampus in memory since it is involved in the same tasks as the hippocampus (Cain et al., 2006; Cooper & Mizumori, 2001; Haijima & Ichitani, 2012; Keene & Bucci, 2009; Kwapis et al., 2015; Pothuizen et al., 2010; Vann & Aggleton, 2005), which is why it is important to fully understand the RSC on an electrophysiological level.

Electrophysiological Properties of RSC

Currently the understanding of the RSC on the electrophysiological level is relatively limited. *In vivo* electrophysiology studies demonstrate that the RSC contains head-direction cells (Chen, Lin, Green, Barnes & McNaughton, 1994; Cho & Sharp, 2001; Jacob, Casali, Spieser, Page, Overington & Jeffery, 2017), and is active during the encoding of navigational cues, the encoding of a reward and its location, and during goal directed navigation (Vedder, Miller, Harrsion & Smith, 2016). An *in vitro* study using extracellular electrophysiology found that stimulation of layer I white matter evoked current sinks in layers II-IV, and VI (Nixima, Okanoya & Kurotani, 2013). From their findings they suggested that the microcircuitry in the RSC allows layer V neurons to integrate thalamic inputs, that are time delayed by layer II/III late-spiking neurons, with the direct inputs of other brain regions (Nixima et al., 2013). The first study to use intracellular electrophysiological techniques reported an inability to induce LTP in the RSC but LTD was achieved (Garden et al., 2009). However, no intrinsic properties were reported.

The only published work that has described intrinsic properties of the RSC reported only two distinct neuronal firing patterns, regular-spiking and late-spiking. Kurotani and colleagues (2013) focused on thoroughly characterizing the late-spiking pyramidal neurons that they found in layer II of the GRS using a number of techniques, including single-cell reverse transcriptase-polymerase chain reaction (RT-PCR). With single-cell RT-PCR, they identified that Kv1.1, Kv1.4, and Kv4.3 channels are highly expressed in these late-spiking layer II GRS pyramidal neurons and pharmacologically blocked these channels during recordings to verify that they were responsible for the late-spiking property (Kurotani et al., 2013). However, the current study establishes the existence of four distinct firing patterns in the GRS. The firing patterns include regular-spiking with a pronounced afterdepolarization (ADP-RS), double-spiking (DS), fast-

spiking (FS), and late-spiking (LS). Although an afterdepolarization (ADP) is not completely unique to ADP-RS neurons, DS and LS neurons also have distinguishable ADPs. Figure 1 and table 2 demonstrate that these populations of cells are distinct in both their firing patterns and their intrinsic properties.

Presently, the mechanism that gives rise to these ADPs in GRS neurons is unknown. However, previous studies suggest that ADP generation is mediated by activation of the phospholipase C (PLC) signaling pathway, and Ca^{2+} influx into the cell (Haj-Dahmane & Andrade, 1997, 1998; Hofmann & Frazier, 2010; Lei et al., 2014; Yan, Villalobos, & Andrade, 2009). As a result, multiple targets for manipulating an ADP have been identified and tested, including group 1 metabotropic glutamate receptors (mGluRs) (Greene, Schwindt, & Crill, 1994; Park et al., 2010), muscarinic receptors (Haj-Dahmane & Andrade, 1998; Hofmann & Frazier, 2010; Yan et al., 2009), and calcium activated non-selective cation channels (Haj-Dahmane & Andrade, 1997; Hofmann & Frazier, 2010; Lei et al., 2014; Yan et al., 2009) and a subclass of these calcium activated non-selective cation channels are permeable to calcium (Okada et al., 1998; Philipp et al., 2000). The current study examined the role that group 1 metabotropic glutamate receptors, mGluR1 & mGluR5, have in mediating the ADP observed in ADP-RS neurons within the GRS.

The ion channels responsible for fast-spiking (FS) GRS neurons is also presently unknown. These cells may be similar to interneurons that have been well characterized in other cortical regions of the brain. Their FS property would thus be mediated by the voltage gated K^+ channels Kv3.1-Kv3.2 (Erisir, Lau, Rudy, & Leonard, 1999; Rudy et al., 1999). The present study also investigated the role of voltage gated K^+ channels Kv3.1-Kv3.2 in promoting the FS property observed in FS neurons within the GRS. Further, the present study morphologically

characterized GRS neurons based upon their firing patterns. Thorough characterization of electrophysiological and morphological properties of neurons in the GRS will add to the foundation for a complete understanding of the RSC.

Method

Subjects

Subjects were adult male Sprague Dawley and F344 rats 2-3 months of age. Rats were maintained in an AAALAC (Association for Assessment and Accreditation of Laboratory Animal Care) accredited facility on a 14-hour light/10-hour dark cycle and housed individually with *ad libitum* access to food and water. Procedures were conducted in accordance with the University of Wisconsin – Milwaukee Animal Care and Use Committee and NIH guidelines.

RSC Slice Preparation

Rats were deeply anaesthetized with isoflurane and an intracardiac perfusion was performed with ice-cold oxygenated sucrose-aCSF (composition in mM: 206 Sucrose, 26 $NaHCO_3$, 10 D-glucose, 2.80 KCl, 2 $MgSO_4 7H_2O$, 1.25 $NaH_2PO_4 H_2O$, 1 $CaCl_2$, 1 $MgCl_2$, .40 Na-ascorbate). Then the brain was quickly removed and placed in ice-cold oxygenated sucrose-aCSF. The brain was then blocked with three dissections, (anterior and posterior sections and a portion of left hemisphere was removed) and coronal brain slices (400 μm) containing the retrosplenial cortex (anteroposterior, -1.80 to -3.80 mm) was cut in oxygenated sucrose-aCSF at ~ 1℃ using a vibrating tissue slicer (VT1200, Leica). Slices were then transferred to a holding chamber (Moyer & Brown, 1998) containing oxygenated aCSF (composition in mM: 124 NaCl, 26 $NaHCO_3$, 20 D-glucose, 2.80 KCl, 2 $MgSO_4 7H_2O$, 1.25 $NaH_2PO_4 H_2O$, 2 $CaCl_2$) at 32-36℃ and was incubated for at least 30 minutes before performing recordings.

Electrophysiological Recordings

An Olympus BX51WI upright microscope outfitted with a submerged recording chamber and equipped with infrared DIC optics was used for visualizing the neuron and patch electrode. Slices were transferred to the chamber where they were perfused at a rate of 2.1 ml/min (maintained at 32-36℃ using an inline temperature controller). Whole cell recordings (WCRs) were made from layers II, III, and V of the anterior portion of granular retrosplenial cortex (anteroposterior, ~ -1.80 to -3.80). For WCRs, electrodes (~4-5 MΩ) were prepared from thin-walled capillary glass and filled with the following solution (in mM): 110 K-gluconate, 20 KCL, 10 Di-Tris-P-Creatine, 10 HEPES, 2 $MgCl_2$, 2 Na_2ATP, 0.3 Na_2GTP, 0.2% Biocytin, pH to 7.3. For experiments requiring synaptic stimulation, FHC concentric bipolar electrodes were used (FHC, Bowdoin, ME, Canada) along with a World Precision Instruments A365 bipolar high voltage isolator (World Precision Instruments Inc., Sarasota, FL). All recordings were obtained in current clamp mode (holding potential -67 ±3 mV) using a HEKA EPC10 amplifier system (HEKA instruments Inc. Bellmore, New York). Data were collected from neurons with a resting membrane potential more negative than -50 mV. Series resistance was fully compensated and consistently monitored to ensure the stability of recording conditions, and cells were only analyzed if the initial series resistance did not change by >30% throughout the recording period. Experiments were controlled by PatchMaster software (HEKA Instruments) running on a PC and data were transferred to a PC using an ITC-16 digital-to-analog converter (HEKA Instruments). The signals were filtered at 2.9 kHz and digitized at 20 kHz using PatchMaster software. Data was analyzed off-line using PatchMaster and Igor Pro software (version 6.37; Wavemetrics). Voltages were not corrected for the liquid-liquid junction potential (approximately +13 mV; Moyer and Brown, 2007).

Intrinsic properties of GRS neurons were studied under current-clamp conditions using the following protocols, which have previously been described (Song, Ehlers, & Moyer, 2015). (1) I-V relationships were obtained from a series of 500 ms current injections (ranging from -300 to +50 pA) and the plateau voltage deflection was plotted against the current amplitude. Neuronal input resistance (R_N) was determined from the slope of the linear fit of the portion of the V-I plot where the voltage sweeps did not exhibit sags or active conductance. Similarly, Tau was defined as 63% of the time until plateau voltage deflection and the average Tau for each neuron was calculated from voltage sweeps that did not exhibit sags or active conductance. The sag ratio during hyperpolarizing membrane responses was expressed as $[(1 - \Delta V_{ss}/\Delta V_{max}) \times 100\%]$, where ΔV_{ss} = MP - V_{ss} and ΔV_{max} = MP - V_{max} (MP is the membrane potential before the current step, V_{ss} is the steady-state potential at the end of the current step, and V_{max} is the peak amplitude during the first 150 ms of the current step). For each neuron, the sag ratio was calculated from current injections of -300, -250, and -200 pA and averaged. (2) Action potential (AP) properties were studied with an ascending series of .5 s or 1 s depolarizing pulses (5 pA increments). At rheobase, neurons could be classified as afterdepolarizing-regular spiking (ADP-RS), double-spiking (DS), fast-spiking (FS), or late-spiking (LS). Cells were classified by firing type based on how the cell responded to suprathreshold current injections. ADP-RS neurons were defined as neurons that, exhibit spike frequency adaptation, fire a single action potential (AP) at rheobase within ~350 ms of a 500 ms current injection, and have a pronounced ADP after each action potential. DS neurons were defined as neurons that fire two action potentials in short succession (~8 ms) at the beginning of the current injection either at rheobase or within 20 pA of rheobase. FS neurons were defined as neurons that, exhibit little to no spike frequency adaptation, display no repetitive burst firing, fire action potentials with short duration (<.5 ms AP

width at half-amplitude), and repolarize rapidly after an AP (Faulkner & Brown, 1999). LS neurons were defined as neurons that, exhibit little to no spike frequency adaptation and delay firing an action potential until the end of the current injection (~700 ms in a 1 s current injection) (Faulkner & Brown, 1999; Moyer, McNay, & Brown, 2002). For all neurons, AP properties were studied from the first spike. I-threshold was defined as the minimum amount of depolarizing current required to evoke an AP from a recorded neuron. AP-threshold was defined as the voltage when dV/dt first exceeded 28 mV/ms (Kaczorowski et al., 2012). The latency to AP was defined as the time to the peak of the first action potential relative to the onset of the current injection. AP-amplitude was measured relative to the AP-threshold, and fast-AHP (fAHP) was also measured relative to AP-threshold; and ADP-amplitude was measured relative to fAHP. For drug experiments, an average ADP-amplitude was calculated pre- and post-drug application by measuring ADP-amplitude at rheobase, and from the first AP in subsequent current injections close to rheobase (within 20 pA). Lastly, $AP_{half\text{-}width}$ was measured as the width at half of the AP amplitude. (3) Post-burst afterhyperpolarization (AHP) was studied after a 50 Hz burst of 10 spikes, each of which was evoked by a 2 ms suprathreshold current injection (three times, at 20 s intervals). After the last action potential, the post-burst AHP was measured at the peak amplitude. (4) Neuronal excitability was assessed by counting the number of spikes evoked in response to a series of 5 s depolarizing steps (range, 0-450 pA; 50 pA increments, 20 s ITI). (5) Firing frequency was assessed by measuring initial and steady state firing frequency from a series of 5 s depolarizing steps (range, 0-725 pA; 25 pA increments, 20 s ITI). Initial firing frequency (IFF) was calculated by first measuring the inter-spike-interval (ISI) between the first and second evoked AP (1^{st} ISI) in the 5 s long current injection. This ISI was then used in the following equation to calculate initial firing frequency: IFF = $1/1^{st}$ ISI ms × 1000 ms/1 s. Steady

state firing frequency (SSFF) was calculated by first measuring the ISI between the first and second evoked AP that occurred after 200 ms of the 5 s current injection. This definition of steady state firing is similar to previous studies assessing firing frequency (e.g., Erisir et al., 1999). This ISI was then used in the following equation calculating steady state firing frequency: SSFF = $1/200_{(ms)}$ ISI ms × 1000 ms/1 s. Both types firing frequencies were calculated for each applicable current injection in the series.

Pharmacological Agents

For pharmacological studies, stock drug solutions were made by adding the appropriate amount of double distilled purified water to achieve the desired concentration for the solution, and then the appropriate stock solution was diluted in aCSF. The following pharmacological agents were used in experiments: 6-cyano-7-nitroquinoxaline-2, 3-dione (CNQX, 10 μm – AMPA receptor antagonist), D-(-)-2-amino-5-phosphonopentanoic acid (D-AP5, 30 μm – NMDA receptor antagonist), (S)-(+)-α-amino-4-carbody-2-methylbenzeneacetic acid (LY367385, 10 μm – mGluR1 antagonist) and 2-methyl-6-(phenylethynyl) pyridine hydrochloride (MPEP, 10 μm – mGluR5 antagonist), tetraethylammonium chloride (TEA, 1mM – K^+ antagonist and selective for a few K^+ channels including Kv3.1-Kv3.2 at low doses, Erisir et al., 1999), all obtained from Tocris (Bio-Techne, Minneapolis, MN).

Biocytin Staining

All neurons were filled with biocytin to confirm the location and perform morphological analysis of cells in the granular retrosplenial cortex. After completion of WCRs, slices were fixed in formalin and kept at 4℃ for at least 1 day and no longer than 10 days before further processing. To visualize neurons labeled by biocytin, the slices were washed with 0.1 M PBS for 5 min (three times). Slices were then incubated in H_2O_2/methanol for 45 min, then another wash

with 0.1 M PBS for 5 min (three times), followed by Triton X-100/BSA for 45 min. Then slices were incubated with 1:500 Streptavidin-Alexa Fluor-488 (Invitrogen) for 120 min in the dark or overnight in 4℃ in the dark. Then slices were washed with 0.1 M PBS for 5 min (three times), and subsequently mounted on slides, coverslipped with DAPI containing Ultra Cruz Mounting Medium (Santa Cruz Biotechonology, Houston TX), and sealed with nail polish.

Neuron Imaging, Reconstruction, and Analysis

The neurons previously processed with Streptavidin-Alexa Fluor-488 were viewed under a fluorescence microscope at 2X and 100X and photographed using an Olympus BX51 upright microscope with attached CCD camera (Olympus microscopy). At 2X, an image of the hippocampus was captured to determine approximate anterior/posterior location of slice. At 100X spines on apical dendrites and basilar dendrites were visualized and 2-4 images were taken to document if spines were present on the dendrites of the neurons. The stained neurons were also viewed under a confocal microscope at 10X to capture a dual channel image (DAPI & Alexa Fluor-488) to determine laminar location of neurons (see figure 2), and both 20X and 100X to capture a Z-stack of stained neurons to render three dimensional images of stained neurons and spines respectively, using an Olympus FV1000 confocal system (Olympus microscopy). The 20X image stacks were then used to reconstruct stained neurons using Neurolucida 360 and subsequent analysis was performed with Neurolucida Explorer (MBF Bioscience, Williston, VT).

Statistical Analyses

For all WCRs and neuronal reconstructions, data was averaged based on the firing type of the cell and are reported as the mean ± standard error of the mean. The overall differences between firing types was examined using one-way and two-way ANOVA using GraphPad Prism

7.00 (GraphPad Software, Inc., La Jolla, CA). For each significant F ratio (0.05 level) Tukey's multiple comparisons test was used to determine specific differences between firing types. Laminar comparisons of LS neurons were made using Welch's t-test and two-way ANOVA; for each significant F ratio (0.05 level) Sidak's multiple comparisons test was used to determine specific differences. For all drug experiments, one-way ANOVA and Sidak's multiple comparisons test was used to evaluate drug effects.

Results

Recordings were made from 130 neurons; 74 were classified as ADP-RS, 11 as DS, 10 as FS, 32 as LS, 1 Regular Spiking (RS), and 2 neurons did not fit into one of the five classifications due to intermittently exhibiting characteristics of multiple classifications. Only 122 neurons were analyzed after excluding 3 ADP-RS, 2 FS, and 1 RS neuron(s) due to a loss in the stability of the recording (large change in series resistance, resting membrane potential, or noise), and the 2 neurons that didn't fit into a classification were also excluded. However, the morphology of the excluded ADP-RS and FS neurons from these recordings was still analyzed. From the 122 neurons analyzed for physiology, a subset of neurons was analyzed for morphology, including 48 ADP-RS, 5 DS, 7 FS, and 25 LS neurons. From this analysis, the laminar location of these neurons was determined, 8 resided in layer II, 19 resided in layer III, and 58 resided in layer V.

The physiology of the four firing types differed on several of their intrinsic cellular properties (see table 2 for full summary), including resting membrane potential, input resistance, post-burst afterhyperpolarization (AHP) peak, latency to action potential (AP), AP half-width, and neuronal excitability. One-way ANOVA revealed a main effect of firing type on resting membrane potential ($F_{(3, 118)} = 6.81$, $p < .01$) and *post-hoc* analysis revealed that LS neurons are

significantly more hyperpolarized than ADP-RS neurons, $p < .01$. Unsurprisingly, a main effect of firing type on input resistance was found ($F_{(3, 118)} = 155.48$, $p < .01$); *post-hoc* analysis revealed that LS neurons have significantly larger input resistance when compared to all other firing types, $p < .01$ (for all comparisons). Further, a main effect of firing type on post-burst AHP peak was found ($F_{(3, 116)} = 4.50$, $p < .01$) and as we expected, *post-hoc* analysis revealed that FS neurons have a significantly smaller post-burst AHP peak when compared to ADP-RS ($p < .05$) and LS ($p < .01$) neurons. Moreover, a main effect of firing type on latency to AP was found ($F_{(3, 118)} = 100.90$, $p < .01$) and predictably, *post-hoc* analysis revealed that LS neurons have a significantly longer latency to AP when compared to all other firing types, $p < .01$ (for all comparisons). Also a main effect of firing type on AP half-width was found ($F_{(3, 118)} = 40.55$, $p < .01$) and *post-hoc* analysis revealed that each firing type is different from every other type: ADP-RS < DS ($p < .01$), ADP-RS > LS ($p < .05$), DS > LS ($p < .01$), FS < ADP-RS, DS & LS ($p < .01$). Lastly, a two way ANOVA on neuronal excitability revealed a main effect of firing type ($F_{(3, 1138)} = 537.8$, $p < .01$), current injection ($F_{(9, 1138)} = 137.4$, $p < .01$), and an interaction effect ($F_{(27, 1138)} = 57.81$, $p < .01$). *Post-hoc* analysis revealed that there are statistically significant differences between firing types in the number of AP's fired from 100-450 pA injected: at 100 pA – ADP-RS, DS < LS; FS < LS ($p < .01$ for all comparisons), at 150 pA – ADP-RS, DS < LS ($p < .01$ for all comparisons), at 200 pA – ADP-RS, DS < LS; ADP-RS, DS < FS ($p < .01$ for all comparisons), at 250 pA – ADP-RS, DS < LS; ADP-RS, DS < FS; FS > LS ($p < .01$ for all comparisons), at 300 pA – ADP-RS, DS < LS; ADP-RS, DS < FS; FS > LS ($p < .01$ for all comparisons), at 350 pA –ADP-RS, DS, LS < FS ($p < .01$ for all comparisons), at 400 pA –ADP-RS, DS, LS < FS ($p < .01$ for all comparisons), at 450 pA –ADP-RS, DS, LS < FS; ADP-RS > LS ($p < .01$ for all comparisons) (see figure 2).

Laminar Analyses

Laminar analysis was executed comparing layer II LS neurons to layer III LS neurons, and comparing the morphology of layer III ADP-RS neurons to layer V ADP-RS neurons. A Welch's t-test revealed several differences between layer II LS neurons and layer III LS neurons (data not shown). Firstly, layer II LS neurons require a significantly larger amount of current to be injected to evoke an AP than layer III LS neurons, $t_{(10.41)} = 2.24$, $p < .05$. Next, layer II LS neurons have a significantly smaller post-burst AHP peak than layer III LS neurons, $t_{(15.49)} = 2.18$, $p < .05$. Layer II LS neurons have a significantly larger number of basilar dendrites and branches than layer III LS neurons, $t_{(18)} = 3.58$, $p < .01$. Similarly, layer II LS neurons have a significantly larger total length of basilar dendrites and branches than layer III LS neurons, $t_{(11.61)} = 3.48$, $p < .01$. Lastly, a two-way ANOVA comparing layer II LS & layer III LS neuron's Sholl analysis revealed a significant effect of distance from the soma ($F_{(50, 969)} = 66.40$, $p < .01$), laminar location ($F_{(1, 969)} = 13.21$, $p < .01$), and an interaction effect ($F_{(50, 969)} = 1.83$, $p < .01$); *post-hoc* analysis revealed that at 20 µm from the soma layer II LS neurons have significantly more intersections than layer III LS neurons ($p < .01$), at 30 µm layer II LS neurons have significantly more intersections than layer III LS neurons ($p < .01$), and at 70 µm layer II LS neurons have significantly more intersections than layer III LS neurons ($p < .01$).

A Welch's t-test revealed several differences between layer III ADP-RS neurons and layer V ADP-RS neurons (data not shown). Firstly, layer III ADP-RS neurons have a significantly larger soma volume than layer V ADP-RS neurons, $t_{(41.59)} = 2.84$, $p < .01$. Similarly, layer III ADP-RS neurons have a significantly larger soma surface area than layer V ADP-RS neurons, $t_{(18.98)} = 3.23$, $p < .01$. Next, a two-way ANOVA comparing Sholl data from layer III ADP-RS & layer V ADP-RS neurons revealed a significant effect of distance from the soma ($F_{(50, 2142)} =$

19.03, $p < .01$) and laminar location ($F_{(1, 2142)} = 6.57$, $p < .05$). However, *post-hoc* analysis revealed that there are no statistically significant differences between layer III ADP-RS and layer V ADP-RS neurons.

Morphology

Afterdepolarizing Regular-Spiking Neurons

All 74 neurons classified as ADP-RS neurons were identified as pyramidal at the time of the recording and 48 were later verified as such with confocal microscopy. Of the 74 ADP-RS neurons, 3 were found to reside in layer III (16% of sample from layer III) and 45 in layer V (78% of sample from layer V). Only the cell body was visible in 4 of the 48 neurons processed for morphological analysis, thus only 44 ADP-RS neurons were reconstructed. All 44 ADP-RS neurons that were reconstructed displayed a long primary apical dendrite that projected to layer I of the GRS, and the tufts included numerous bifurcations in all but one case. Similarly, all reconstructed ADP-RS neurons displayed numerous basilar dendrites with many bifurcations (see figure 3-A). Of the 42 neurons that could be visualized at 100X (2 neurons were too deep in the tissue to be visualized), 41 of them had numerous spines on both their apical and basilar dendrites (see figure 4-A), while 1 neuron did not have any visible spines on its apical or basilar dendrites.

Double-Spiking Neurons

All 11 neurons classified as DS neurons were identified as pyramidal at the time of the recording and 5 were later verified as such with confocal microscopy. Of the 11 DS neurons, 5 were verified to reside in layer V (9% of sample from layer V). Only the cell body was visible in 1 of the 5 neurons processed for morphological analysis, thus only 4 DS neurons were reconstructed. All 4 DS neurons that were reconstructed displayed a long primary apical dendrite

that projected to layer I of the GRS, and all the tufts included numerous bifurcations. Similarly, all reconstructed DS neurons displayed numerous basilar dendrites with many bifurcations (see figure 3-B). All 4 neurons that could be visualized at 100X had numerous spines on both their apical and basilar dendrites (see figure 4-B).

Fast-Spiking Neurons

All 11 neurons classified as FS neurons were identified as non-pyramidal at the time of the recording, and 4 were later verified as such with confocal microscopy. Of the 11 FS neurons, 7 were verified to reside in layer V (12% of sample from layer V). Only the cell body was visible in 1 of the 5 neurons processed for morphological analysis, thus only 4 FS neurons were reconstructed. All 4 FS neurons that were reconstructed did not have a clear apical dendrite and had many basilar dendrites projecting in all directions (see figure 3-C). All 4 neurons that could be visualized at 100X did not have any visible spines on their basilar dendrites (see figure 4-C).

Late-Spiking Neurons

Of the 32 neurons classified as LS neurons, all were identified as pyramidal at the time of the recording and 21 were later verified as such with confocal microscopy. LS neurons were found in layers II, III, and V, with 8 recorded cells in layer II (100% of sample from layer II), 16 recorded cells in layer III (84% of sample from layer III), and 1 recorded cell in layer V (2% of sample from layer V). Only the cell body was visible in 4 of the 25 neurons processed for morphological analysis, thus only 21 LS neurons were reconstructed. Of the 21 LS neurons that were reconstructed, 2 displayed a long primary apical dendrite that projected to layer I of the GRS, and the tufts included a few bifurcations, but the other cells bifurcated early and had relatively simple tufts. Similarly, all reconstructed LS neurons exhibited few basilar dendrites with modest bifurcations (see figure 3-D). Of the 15 neurons that could be visualized at 100X (6

neurons were too deep in the tissue to be visualized), 15 of them had a few spines on their apical dendrites and 14 had a few spines on their basilar dendrites, while 1 neuron did not have any visible spines on its basilar dendrites. LS neurons did appear to have less spines overall than ADP-RS and DS neurons, but no quantification was performed (see figure 4-A, B & C).

Morphological Analyses

The 3-D reconstructions of neurons in Neurolucida-360 allowed us to perform branched structure analysis and Sholl analysis of neurons based on cell firing type. However, the biocytin staining consistently poorly labeled axonal arborization often only staining the initial segment of the axon. Although axonal analysis was still performed, the results should not be interpreted as conclusive.

First, no statistically significant differences were found between firing types in the analysis of soma volume, total number of axon bifurcations, and total length of axon and bifurcations (see table 3). However, statistical trends were identified in soma volume (ADP-RS > LS $p = .06$), total number of apical dendrite branches (DS > LS $p = .08$), and total length of basilar dendrites and branches (DS > LS $p = .07$). A one-way ANOVA revealed statistically significant main effects of cell firing type on other measures. A statistically significant main effect of firing type on soma surface area was found ($F_{(3, 70)} = 4.52$, $p < .01$) and unsurprisingly, *post-hoc* analysis revealed that ADP-RS neurons have a significantly larger soma surface area than LS neurons ($p < .01$) (see figure 4-A). A statistically significant main effect of firing type on total number of apical dendrite branches was found ($F_{(2, 66)} = 14.85$, $p < .01$), and *post-hoc* analysis revealed that ADP-RS neurons have a significantly greater total number of apical dendrite branches than LS neurons ($p < .01$) (see figure 4-B). Similarly, a statistically significant main effect of firing type on total length of the apical dendrite and its branches was found ($F_{(2, 66)}$

= 6.38, $p < .01$), and *post-hoc* analysis revealed that ADP-RS neurons have a significantly larger total length of their apical dendrite and branches than LS neurons ($p < .01$) (see figure 4-B). Next, a statistically significant main effect of firing type on total number of basilar dendrites and branches was found ($F_{(3, 70)} = 32.18$, $p < .01$). *Post-hoc* analysis revealed that ADP-RS neurons have a significantly greater total number of basilar dendrites and branches than FS neurons ($p < .05$) and LS neurons ($p < .01$), and DS neurons have a significantly greater total number of basilar dendrites and branches than LS neurons ($p < .01$) (see figure 4-C). Similarly, a statistically significant main effect of firing type on total length of basilar dendrites and branches was found ($F_{(3, 70)} = 12.91$, $p < .01$), and *post-hoc* analysis revealed that ADP-RS neurons have a significantly larger total length of basilar dendrites and branches than LS neurons ($p < .01$) (see figure 4-C). Lastly, a two-way ANOVA revealed a significant effect of distance from the soma ($F_{(50, 3570)} = 33.19$, $p < .01$), firing type ($F_{(3, 3570)} = 134.79$, $p < .01$), and an interaction effect ($F_{(150, 3570)} = 2.91$, $p < .01$). *Post-hoc* analysis revealed that at 20 µm from the soma ADP-RS neurons have significantly more intersections than LS neurons ($p < .01$), at 30 µm ADP-RS & DS neurons have significantly more intersections than LS neurons ($p < .01$ for both comparisons), from 40 µm to 140 µm ADP-RS & DS neurons have significantly more intersections than FS & LS neurons ($p < .05$ for all comparisons), from 150 µm to 170 µm ADP-RS & DS neurons have significantly more intersections than LS neurons ($p < .05$ for all comparisons), and from 180 µm to 290 µm ADP-RS neurons have significantly more intersections than LS neurons ($p < .05$ for all comparisons) (see figure 5).

Pharmacology Experiments

Synaptic Blockade

To determine if the ADP and FS firing properties are intrinsic to ADP-RS and FS neurons respectively, the hypothesis that ionotropic glutamatergic synaptic input doesn't contribute to their respective firing properties observed at rheobase was tested. This was done by first positioning a concentric bipolar electrode in the surrounding tissue (~100-250 μm from the neuron) and established a synaptic connection with the recorded neuron (50-200 μA injected). Once a synaptic connection was identified, CNQX (10 μm) & D-AP5 (30 μm) were both bath applied in aCSF for 20-minutes. To verify that the bath applied pharmacological agents were blocking synaptic input to the recorded neuron, the previously established synaptic connection was tested. If electrical stimulation did not yield an EPSP the pharmacological agents were considered to be blocking synaptic input and the firing pattern of the recorded neuron was reassessed and specific properties for each firing type were analyzed. Four ADP-RS neurons were selected for this experiment, and two of the four were excluded from analysis due to a large change in resting membrane potential or input resistance. A one-way ANOVA on ADP-amplitude revealed a main effect of aCSF ($F_{(3, 11)} = 4.98$, $p < .05$). However, *post-hoc* analysis did not reveal any statistically significant differences (see figure 6). For FS neurons, one cell was selected for the experiment, and both initial and steady state spike frequency was assessed, given that FS neurons display high frequency firing. The same bath application of CNQX and D-AP5 seemed to result in a slight increase in both initial and steady state spike frequency at lower current injections (see figure 7). Although, this experiment has only been done with one cell, thus no statistical analysis was performed.

Specific Channel Blockers

The ADP firing property was further examined by assessing whether blocking group 1 metabotropic glutamate receptors, mGlur1 & mGlur5, would abolish the ADP in GRS neurons, as has previously been reported in other brain regions (Greene, Schwindt, & Crill, 1994; Park et al., 2010). Once a neuron was identified as ADP-RS, LY367385 & MPEP were bath applied for 20 minutes with a concentration of 10 μm or 100 μm. Four cells were selected for this experiment and 2 of the cells received a concentration of 10 μm and the other 2 cells received 100 μm of LY367385 & MPEP. The firing pattern of the recorded neuron was then reassessed and the ADP-amplitude was analyzed. A one-way ANOVA revealed a statistically significant main effect of aCSF on ADP-amplitude ($F_{(2, 35)} = 30.61$, $p < .01$). *Post-hoc* analysis revealed that bath application of LY367385 & MPEP at two concentrations, 10 μm and 100 μm, significantly reduced ADP-amplitude at both concentrations ($p < .01$ both comparisons) but the concentrations didn't significantly differ in their effect ($p = .1$) (see figure 8). However, in all four experiments the ADP wasn't completely abolished (reduction in ADP-amplitude ~30%). The high frequency spiking property observed in FS neurons was also examined. This was done by assessing whether bath application of TEA (1 mm) would cause the recorded FS neuron to display decreased initial and steady state spike frequency, as has previously been reported in other brain regions (Erisir et al., 1999; Rudy et al., 1999). After the 20-minute bath application of 1 mm of TEA, the recorded FS neuron displayed a decreased fast AHP (see figure 9-C & E), required higher current injections to begin firing, and required a higher holding current to rest at -67 mV. It also displayed a decreased initial firing frequency that subsided at higher current injections and a persistent decrease in steady state firing (see figure 9), which is consistent with previous

findings (Erisir et al., 1999; Rudy et al., 1999). However, the experiment has only been conducted with one cell, thus no statistical analysis was performed.

Discussion

The one previous description of GRS neuronal firing properties only reported RS and LS neurons (Kurotani et al., 2013). However, the current study found four distinct firing patterns, including ADP-RS, DS, FS, and LS neurons. The four firing types were assessed on several intrinsic physiological and morphological measures which will be further discussed in the following section.

Four Firing Types in Rat Granular Retrosplenial Cortical Neurons

Although the four neuronal firing patterns are easily distinguishable from each other, several differences in their intrinsic membrane properties was found. The intrinsic action potential properties (assessed at rheobase), and neuronal excitability differed across firing types, which further corroborates the conclusion that there are four distinct neuronal firing patterns in the GRS. LS neurons have a significantly more hyperpolarized resting membrane potential than ADP-RS neurons, have a significantly larger input resistance than all other neurons, and have a significantly longer time constant than all other neurons. While LS neurons require significantly less current to be injected to fire an action potential ($I_{threshold}$), they have a comparable AP threshold to ADP-RS and DS neurons. However, FS neurons require significantly more current to be injected to fire an action potential and have a higher AP threshold than all other neurons. Unsurprisingly LS neurons have a significantly longer latency to first AP than all other neurons. The other difference in rheobase properties that contribute to distinguishing these cells from each other, is that each firing type has a significantly different AP half-width than every other firing type: in ascending order, FS neurons, LS neurons, ADP-RS neurons, and DS neurons. See table 2

for full summary of intrinsic electrophysiological properties. Lastly, the differences in neuronal excitability (as measured by mean number of spikes in response to ascending current injections) are not surprising (see figure 2). Due to large input resistance, low $I_{threshold}$ and repetitive firing, LS neurons are the most excitable neurons at 100 pA and are overall more excitable than ADP-RS and DS neurons. However, due to their non-accommodating nature, FS neurons are overall the most excitable neurons, firing 963 ± 158.6 AP's during the 5 s current injection of 450 pA. Overall, the multitude of electrophysiological differences found between these neurons based on their firing pattern makes it clear that these are indeed distinct populations of cells in the GRS. This will inform future thinking about how the RSC processes information as a whole and will be discussed in more detail later.

In addition to differences in firing patterns, these neurons differed in various morphological properties (see table 3 for full summary). ADP-RS neurons were found to reside in layers III and V, DS and FS neurons in layer V, and LS neurons were primarily found in layer II and III, but one was found in layer V. All ADP-RS, DS, and LS neurons were pyramidal, while all FS neurons were non-pyramidal (see figure 3). Similarly, all but one ADP-RS and all DS neurons were spiny while all FS neurons were non-spiny, and, with one exception, all LS neurons did have spines, but did appear to have less spines than ADP-RS and DS neurons (see figure 4). However, no spine quantification was performed due to an inability to verify consistent staining. Overall, ADP-RS and DS neurons have complex morphology with a long apical dendrite with lots of branching, and many basilar dendrites with quite a bit of branching. FS neurons have no distinguishable apical dendrite or axon, but have modest basilar dendritic branching. LS neurons are overall less complex with less soma surface area, less apical and basilar dendritic branching, and a smaller total length of apical and basilar dendritic branches

when compared to ADP-RS neurons. DS neuronal measures are like those of ADP-RS neurons and would thus likely display the same significant differences from LS neurons if more data could be added. These differences in complexity are also reflected by Sholl analysis (see figure 6).

Laminar Differences

Laminar analyses were conducted comparing the physiology and morphology of layer II & III LS neurons and the morphology of layer III & V ADP-RS neurons. The results indicate that layer II LS neurons require a larger amount of current to be injected to evoke an AP, and have a smaller post-burst AHP than layer III LS neurons. These two differences work in opposition to determining overall neuronal excitability, thus it seems unlikely that either population of cells is more or less excitable than the other. We also found that layer II LS neurons have a larger number of basilar dendrites and branches, and a larger total length of basilar dendrites than layer III LS neurons. Similarly, the results of our Sholl analysis indicate that layer II LS neurons have more intersections than layer III LS neurons at multiple distances from the soma. These differences could be due to the fact that layer II of the GRS is much more densely packed with cells than layer III (Ichinohe et al., 2008; Wyss, Van Groen & Sripanidkulchai, 1990), and thus these cells develop more dendrites due to the higher cell density. No other differences were found between layer II and layer III LS neurons. Lastly, the analyses determined that layer III ADP-RS neurons have a larger soma volume and surface area than layer V ADP-RS neurons. No other differences were found between layer III and layer V ADP-RS neurons.

Intrinsic Afterdepolarizing & Fast-Spiking Properties

In the current study, two pharmacology experiments were used to further study the ADP and FS properties observed in ADP-RS and FS neurons within the GRS. Using the synaptic

blockers CNQX and D-AP5, the hypothesis that ionotropic glutamatergic synaptic input does not influence the ADP property observed in ADP-RS neurons was tested. In both experiments the synaptic blockers did not have a significant effect on ADP-amplitude, which suggests that ionotropic glutamatergic synaptic input doesn't influence the ADP property observed in ADP-RS neurons. However, this experiment should be replicated with more cells. Next, the same experiment in one FS neuron was conducted and a slight increase in initial and steady state spike frequency at lower current injections was observed, but this did not persist at higher current injections (see figure 7-A & B). Although a decisive conclusion cannot be drawn from one experiment, the repetitive firing observed in FS neurons doesn't seem to be due to ionotropic glutamatergic synaptic input.

Next, specific channel blockers were used to study the underlying mechanisms mediating the ADP property observed in ADP-RS neurons in the GRS. We first tested the hypothesis that the ADP would be abolished following blockade of group 1 metabotropic glutamate receptors, mGlur1 & mGlur5, as has previously been observed in other brain regions (Greene et al., 1994; Park et al., 2010). First, a concentration of 10 μm for both LY367385 & MPEP was tested in two experiments. We found a significant reduction in ADP-amplitude, but unlike previous reports, the ADP wasn't completely abolished. Next, a concentration of 100 μm for both LY367385 & MPEP was tested in two experiments, and again we found a significant reduction in ADP-amplitude, but the ADP still wasn't completely abolished (see figure 8). One possible explanation for our results is that a Ca^{2+}-activated non-selective cation current (I_{CAN}) may be contributing to the ADP. However, there are several different channels that could be mediating this current. Transient receptor potential (TRP) channels are thought to contribute to the I_{CAN} underlying the ADP observed in multiple brain regions (Fowler, Sidiropoulou, Ozkan, Phillips & Cooper, 2007; Yan,

Villalobos & Andrade, 2009). Previous studies have found that the ADP observed in layer V prefrontal cortical neurons is mediated by I_{CAN} (Haj-Dahmane & Andrade, 1997, 1998) and that blockade of this current with bath application of flufenamic acid (calcium-activated chloride channel blocker) reduced ADP-amplitude but didn't abolish it (Lei et al., 2014). Similarly, blockade of transient receptor potential melastatin 4 (TRPM4) channels reduced ADP-amplitude but didn't abolish it (Lei et al., 2014). Thus, it seems likely that the ADP observed in GRS neurons is mediated by multiple currents and multiple channels/receptors.

Lastly, TEA was used to study the repetitive firing property observed in FS neurons within the GRS, and we found that bath application of TEA had several effects. The recorded FS neuron displayed a smaller fast-AHP (see figure-9 C & E), required a larger holding current to rest at -67 mV (our standard recording voltage), required larger current injections to begin firing, and lastly a decreased initial and steady state firing frequency was observed (see figure 9). Although, at higher current injections the initial firing frequency matched the initial firing frequency observed before the bath application of TEA. These observations, and the fact that this experiment has only been conducted once, make it impossible to draw definitive conclusions. Still, the decrease in firing frequency observed is consistent with previous findings (Erisir et al., 1999; Rudy et al., 1999).

Functional Implications

The diversity of firing patterns in the GRS suggests that it is a region capable of dynamic information processing and higher-order association, similar to the perirhinal cortex (PR) (Faulkner & Brown, 1999; Moyer, McNay & Brown, 2002). Likewise, studies examining the function of the RSC using an associative learning task support this notion (Corcoran, Leaderbrand & Radulovic, 2013; Kwapis et al., 2014; Kwapis et al., 2015; Robinson et al.,

2012). The RSC may perform these computational functions with it numerous connections to regions such as the prefrontal cortex, cingulate cortex, temporal lobe, para-hippocampal region, hippocampal formation, parietal cortex, thalamus, rhinal cortices, and visual cortices (Aggleton et al., 2012, 2014; Burwell & Amaral, 1998; Czajkowski et al., 2013; Kobayashi & Amaral, 2003, 2007; Miyashita & Rockland, 2007; Morris et al., 1999; Oda et al., 2014; Prasad & Chudasama, 2013; Seltzer & Pandya, 2009; Shibata et al., 2004; Shibata & Naito, 2008: Shibata et al., 2009; Sugar et al., 2011; van Groen & Wyss, 1990, 1992, 2003; Vann et al., 2009; Vogt & Miller, 1983; Wilber et al., 2015). In addition, studies have found functionally important connections between the RSC and other regions. For example, lesioning the ATN reduces spine density (Harland et al., 2014) and immediate early gene expression (Jenkins et al., 2004) in the superficial layers II/III of the RSC, where LS neurons are primarily found. Furthermore, layer V of the RSC provides excitatory input to the medial entorhinal cortex (MEC) (Czajkowski et al., 2013) and the posterior secondary motor cortex (M2) (Yamawaki Radulovic & Shepherd, 2016), as well as receives excitatory input from the posterior secondary motor cortex. In layer V ADP-RS neurons are the most ubiquitous pyramidal neurons, and as a result are likely the cells that provide excitatory input to the MEC and M2 (Czajkowski et al., 2013; Yamawaki et al., 2016).

The ADP property is interesting in that it gives ADP-RS neurons the ability to increase their firing rate, and thus at higher current injections they often display firing patterns similar to DS neurons. It is likely that DS neurons are similar to ADP-RS neurons in their makeup of somatic ion channels since they too display the ADP property. However, they probably have a higher concentration of the receptors and channels that mediate the ADP property which enables the cells to fire doublets. Support for this idea comes from a study that induced an ADP in hippocampal CA1 neurons with bath application of DHPG, a group 1 mGluR agonist (Ireland &

Abraham, 2002). This study suggests that the firing patterns of cells isn't fixed since simple stimulation of receptors produced a unique firing pattern (Ireland & Abraham, 2002), which supports the idea that that DS neurons may be a permutation of ADP-RS neurons with a higher concentration of receptors and channels that mediate the ADP found in GRS neurons.

The study by Ireland and Abraham (2002) also reported that bath application of DHPG made the CA1 neurons more excitable, which supports the assertion that the ADP found in GRS neurons likely makes the cells more excitable than regular-spiking (RS) neurons with no ADP. Consequently, ADP-RS and DS neurons may be more equipped than RS neurons to meaningfully encode a sudden influx of information with little to no loss of detail. A sudden influx of information into the RSC may be due to fluctuations in one's environment. Since it's well established that the RSC is important for contextual memory (Corcoran et al., 2011; Keene & Bucci, 2008a; Keene & Bucci, 2008b; Keene & Bucci, 2008c) and spatial navigation (Cain et al., 2006; Cooper & Mizumori, 2001; Keene & Bucci, 2009; Pothuizen et al., 2010; Vann & Aggleton, 2005), the region likely participates in monitoring environmental changes. Additionally, the ADP property in the GRS may serve a role in working memory, similar to the PFC as both regions are important for working memory (Funahashi, 2017; Pothuizen et al., 2010). The ADP in PFC contributes to persistent firing induction at the neuronal level (Sidiropoulou et al., 2009; Sidiropoulou & Poirazi, 2012; Papoutsi, Sidiropoulou, Cutsuridis & Poirazi, 2013) which is thought to be the biophysical mechanism of working memory (Sidiropoulou et al., 2009).

The inputs of ADP-RS neurons are likely modulated by GABAergic projections from the hippocampus that terminate in layer I (Miyashita & Rockland, 2007), where ADP-RS neurons have complex apical dendritic tufts. Moreover, their output is likely modulated by non-pyramidal

FS neurons found in layer V, and even though FS neurons in the GRS haven't been confirmed to be interneurons, non-pyramidal FS neurons in other brain regions are GABAergic interneurons (Cauli et al., 1997; Freund & Buzaski, 1996; Kawaguchi, 1995; Kawaguchi & Kubota, 1997). Additionally, although the layer and electrophysiological characteristics weren't specified, the RSC does have populations of cholecystokinin (CCK) and parvalbumin (PV) expressing GABAergic neurons, with PV expressing neurons being more numerous (Whissell, Cajanding, Fogel & Kim, 2015). Other studies have reported higher concentrations of interneurons in superficial layers of GRS (Murakami, Ishikawa & Sato, 2013; Salaj, Druga, Cerman, Kubova & Barinka, 2015) but confirmed the presence of calretinin and PV immunoreactive neurons in all layers (Salaj et al., 2015), hence it is likely that GRS non-pyramidal FS neurons are GABAergic interneurons. DS neurons display nearly identical morphology to ADP-RS neurons, and thus, are also likely modulated by GABAergic projections from the hippocampus that terminate in layer I and non-pyramidal layer V FS neurons in the same way as ADP-RS neurons.

The way in which FS neurons likely provide inhibition to layer V ADP-RS and DS neurons to balance cortical activity is similar to the way in which the neocortex, (Haider, Duque, Hasenstaub & McCormick, 2006; Sanchez-Vives & McCormick, 2000; Shu, Hasenstaub & McCormick, 2003) and mPFC are thought to operate (Insel & Barnes, 2015). A recent study used *in vivo* recordings to examine how RS, FS, and burst-spiking (BS) neurons differentially activate in mPFC during a radial arm maze. They found that RS neurons were active during exposure to the behavioral context and firing fields tended to cluster around reward sites, indicating the cells were supporting the association between reward and spatial location (Insel & Barnes, 2015). The FS neuron's activity was associated with movement and the accompanying sensory stimulation, suggesting that the FS neurons were modulating influx of sensory information to the mPFC

(Insel & Barnes, 2015). Lastly, the BS neurons were heterogeneous and overall did not show clustered firing fields, indicating that they were generally less selective than RS neurons (Insel & Barnes, 2015). Although *in vivo* recordings in the RSC haven't examined the role of specific firing patterns, they did find that the RSC's activity during spatial tasks suggests that it's encoding navigational information that's goal directed (Vedder et al., 2016), and head-direction signals that are associated to landmarks (Jacob et al., 2017).

It's more difficult to presume the function of LS neurons given their heterogeneity in phenotype within other brain regions, such as superior colliculus (Saito & Isa, 2000), basolateral amygdala (Washburn & Moises, 1992), amygdala central nucleus (ACe) (Martina, Royer & Pare, 1999), hippocampus CA1 (Storm, 1988; Wu & Barish, 1999), neostriatum (Nisenbaum, Xu & Wilson, 1994; Nisenbaum & Wilson, 1995), visual and somatosensory cortex (Chu, Galarreta & Hestrin, 2003), PR (Beggs, Moyer, McGann & Brown, 2000; McGann, Moyer & Brown, 2001; Moyer et al., 2002), and frontal cortex (Kawaguchi, 1995; Kawaguchi & Kubota, 1997). For example, hippocampal CA1 neurons require strong hyperpolarizing prepulses to display the LS property, but neurons in neostriatum (Nisenbaum et al., 1994; Nisenbaum & Wilson, 1995), PR (Beggs et al., 2000; McGann et al., 2001; Moyer et al., 2002), and GRS, reported here, exhibit this LS property when depolarized from rest. Even cortical LS neurons are heterogeneous across regions. For example, LS neurons in layer I of visual and somatosensory cortex are GABAergic and provide inhibition to neurons and distal dendrites (Chu et al., 2003), LS neurons in layer VI of PR vary greatly in their morphology (McGann et al., 2001), and LS neurons in layer V of PR delay their firing for ~7-12 s, longer than most other reports, (Moyer et al., 2002). LS neurons in the GRS appear to be a relatively homogeneous population of neurons given that they are all pyramidal and appear to be primarily located in superficial layers of the GRS, II and III. These

LS neurons may play a role in several different computational functions, such as encoding information over long time intervals, and/or integrating synaptic input to form a representation of a context (Beggs et al., 2000; Kurotani et al., 2013; McGann et al., 2001; Moyer et al., 2002; Tieu et al., 1999). Both of these theoretical functions for LS neurons are supported by studies demonstrating that the RSC is involved in associative learning (Corcoran et al., 2013; Kwapis et al., 2014; Kwapis et al., 2015; Robinson et al., 2012), which requires encoding information over long time intervals (i.e. trace interval), and both contextual memory (Corcoran et al., 2011; Keene & Bucci, 2008a; Keene & Bucci, 2008b; Keene & Bucci, 2008c) and spatial learning (Cain et al., 2006; Cooper & Mizumori, 2001; Keene & Bucci, 2009; Pothuizen et al., 2010; Vann & Aggleton, 2005), which requires integrating synaptic input to form a representation of a context. In addition, an *in vitro* study using extracellular electrophysiology suggested that the microcircuitry in the RSC allows layer V neurons to integrate thalamic inputs, that are time delayed by layer II/III LS neurons, with direct inputs from other brain regions (Nixima et al., 2013).

Future Directions

An unanswered question from this work is what other receptors or channels are contributing to the ADP observed in GRS neurons. As previously discussed, a Ca^{2+}-activated non-selective cation current (I_{CAN}) may be contributing the ADP (Haj-Dahmane & Andrade, 1997, 1998), and the likely channel mediating this is the transient receptor potential (TRP) channel (Fowler et al., 2007; Yan et al., 2009). An important first step would be to examine the effect of blocking I_{CAN} with bath application of flufenamic acid and observing the effect on ADP-amplitude. We would likely see a reduction in ADP-amplitude, similar to previous studies examining the effects of flufenamic acid on ADP-amplitude (Lei et al., 2014). Similarly,

blockade of TRPM4 would likely reduce ADP-amplitude but not abolish it (Lei et al., 2014). Conversely, once the mediators of the ADP in GRS neurons are determined, it would be interesting stimulate these receptors and channels. An ADP has previously been induced in hippocampal CA1 neurons (Ireland & Abraham, 2002), which suggest that firing patterns are plastic. Stimulation of receptors and channels that mediate the ADP in an ADP-RS neuron may convert the cell into a DS neuron. Another exciting future direction would be to study learning associated changes in intrinsic excitability within the GRS. Since the RSC is clearly important for learning and memory (see review, Todd & Bucci, 2015), learning associated changes likely occur within the region.

Conclusions

The current study established the presence of four distinct firing patterns within GRS neurons, and further demonstrated that these are distinct populations of neurons by characterizing their intrinsic electrophysiological and morphological properties. ADP-RS and DS neurons within the GRS may be supporting contextual and spatial memory/navigation (Cain et al., 2006; Cooper & Mizumori, 2001; Corcoran et al., 2011; Keene & Bucci, 2008a; Keene & Bucci, 2008b; Keene & Bucci, 2008c; Keene & Bucci, 2009; Pothuizen et al., 2010; Vann & Aggleton, 2005) since similar neurons in the mPFC are known to be active during a spatial task (Insel & Barnes 2015). The ADP-RS and DS neurons may also play a role in the working memory that the GRS supports (Pothuizen et al., 2010), since the ADP in PFC neurons is thought to be the biophysical mechanism underlying PFC dependent working memory (Sidiropoulou et al., 2009; Sidiropoulou & Poirazi, 2012; Papoutsi, Sidiropoulou, Cutsuridis & Poirazi, 2013). FS neurons in the GRS are likely interneurons that modulate the circuits they are a part of (Cauli et al., 1997; Freund & Buzaski, 1996; Kawaguchi, 1995; Kawaguchi & Kubota, 1997; Murakami et

al., 2013; Salaj et al., 2015; Whissell et al., 2015), which may be particularly important when the GRS is supporting spatial tasks (Insel & Barnes. 2015). LS neurons in the PR are thought to play a role in encoding information over long time intervals and/or integrating synaptic input to form a rich representation of a context (Beggs et al., 2000; Kurotani et al., 2013; McGann et al., 2001; Moyer et al., 2002; Tieu et al., 1999), and LS neurons within the GRS likely perform these computational functions as well (Nixima et al., 2013). The present study also investigated the mechanism underlying the ADP observed in ADP-RS neurons within the GRS. Our findings indicate that the ADP observed in ADP-RS neurons within the GRS are intrinsic to the cells and that the ADP is mediated by multiple receptors and/or channels, which includes mGluR1 and mGluR5. Likewise, the mechanism underlying fast-spiking observed in FS neurons within the GRS was investigated. Our findings indicate that the fast-spiking property is intrinsic to the cells and that Kv3.1-Kv3.2 channels play an important role in the high firing frequency that these neurons typically achieve. These findings provide a foundation for understanding how the RSC may function to perform its important functions as well as shed light on how it may interact with other interconnected brain regions.

Table 1

Learning-Associated Intrinsic Plasticity

Brain Region	Behavioral Task	Electrophysiological Properties	Intrinsic Excitability	Citation
Infralimbic PFC				
	Delay Fear Conditioning	↑ slow AHP & spike-frequency adaptation	↓ Excitability	(Santini et al., 2008)
	Extinction of Conditioned Fear	↓ fast AHP	↑ Excitability	(Santini et al., 2008)
	Trace Fear Conditioning	↓ medium AHP & spike-frequency adaptation	↑ Excitability	(Song et al., 2015)
Prelimbic PFC				
	Trace Fear Conditioning	↓ input resistance	↓ Excitability	(Song et al., 2015)
Piriform Cortex				
	Olfactory Discrimination	↓ AHP & spike-frequency adaptation	↑ Excitability	(Cohen-Matsliah et al., 2009; Saar et al., 1998)
Hippocampus				
	Trace Eyeblink Conditioning	↓ AHP & spike-frequency adaptation	↑ Excitability	(Moyer et al., 1996; Thompson et al., 1996)
	Morris Water Maze	↓ AHP	↑ Excitability	(Oh et al., 2003)
	Trace & Context Fear Conditioning	↓ AHP & spike-frequency adaptation	↑ Excitability	(Kaczorowski & Disterhoft, 2009; McKay et al., 2009; Song et al., 2012)
	Olfactory Discrimination	↓ AHP & spike-frequency adaptation	↑ Excitability	(Zelcer et al., 2006)
Amygdala				
	Delay Fear Conditioning	↓ AHP & spike-frequency adaptation	↑ Excitability	(Sehgal et al., 2014)
	Olfactory Discrimination	↓ AHP & spike-frequency adaptation	↑ Excitability	(Motanis et al., 2014)
	Olfactory Fear Conditioning	↑ spike-frequency adaptation	↓ Excitability	(Motanis et al., 2014)

Table 2

Intrinsic Cellular Properties

	ADP-RS (71)	**DS (11)**	**FS (8)**	**LS (32)**
Membrane Properties				
RMP (mV)	–65.7 ± 0.5	–66.2 ± 1	–66 ± 1.7	–70.2 ± 1 #
R_N (MΩ)	127.1 ± 7.3	122.1 ± 12.8	113.6 ± 11.7	470.3 ± 20.7 # § †
Tau (ms)	39.1 ± .8	42.3 ± 2.1	32.6 ± 2.8 # §	50 ± 0.7 # § †
Sag (%)	0.33 ± 0.04	0.14 ± 0.02	0.26 ± 0.18	0.06 ± 0.01 #
Post-Burst AHP				
AHP_{peak} (mV)	–3.4 ± 0.1	–3.3 ± 0.1	–1.9 ± 0.3 # *	–3.7 ± 0.3
AHP_{peak} (ms)	82.5 ± 9.8	101 ± 12.6	114.2 ± 30.8	177 ± 25.7 #
Rheobase Properties				
$I_{threshold}$ (pA)	85.1 ± 6.4	74.9 ± 6.9	145 ± 16.7 # §	48.2 ± 4.2 # †
$AP_{threshold}$ (mV)	–36.9 ± 0.5	–36.1 ± 1.4	–42.6 ± 1.9 # § *	–36.8 ± 0.7
Latency to AP (ms)	214.7 ± 11.4	206.1 ± 24.7	102.1 ± 36.8	643.9 ± 32.1 # § †
$AP_{amplitude}$ (mV)	91.2 ± 1	88.4 ± 2.1	84.2 ± 5.6	77 ± 1.8 # §
fAHP (mV)	14.2 ± 0.4	9.6 ± 1	13.4 ± 10.5	19.6 ± 0.5 # §
mAHP (mV)	20.2 ± 0.4	20.4 ± 1.1	n/a	19.6 ± 0.5
$ADP_{amplitude}$ (mV)	3.5 ± 0.2	2.5 ± 0.5	n/a	4.6 ± 0.3 # §
$AP_{half\text{-}width}$ (μs)	466.6 ± 8.8 § † *	550.9 ± 31 † *	192.8 ± 28.5 *	422.4 ± 11.2

Note. Data are mean ± SE for number of cells in parentheses. A one-way ANOVA was used to compare each firing type against the other for each of the membrane properties, post-burst AHP and rheobase properties. A Tukey HSD *post-hoc* test was used for multiple comparisons. Significantly different from LS (*, $p < .05$). Significantly different from ADP-RS (#, $p < .05$). Significantly different from DS (§, $p < .05$). Significantly different from FS (†, $p < .05$).

Table 3

Intrinsic Morphological Properties

	ADP-RS (44)	DS (4)	FS (5)	LS (21)
Morphological Measurements				
Soma Volume (μm^3)	2605.7 ± 589.6	1247.1 ± 334.8	895.3 ± 280.6	543.3 ± 70.3
Soma Surface Area (μm^2)	785.2 ± 89.3 *	544.7 ± 102.5	425 ± 87.9	339.1 ± 33.6
Apical Dendrite & Branches Total	37.6 ± 3 *	33.8 ± 4.8	n/a	13.5 ± 1.2
Apical Dendrite & Branches Total Length (μm)	1951.7 ± 259.8 *	1548.2 ± 180.6	n/a	627.7 ± 46.4
Basilar Dendrites & Branches Total	59.8 ± 3.5 *	56.5 ± 6.3 *	33.4 ± 5 #	11.5 ± 1
Basilar Dendrites & Branches Total Length (μm)	2751.1 ± 266.3 *	2350.4 ± 323.7	1541.4 ± 273.5	460 ± 41.1
Axon & Bifurcations Total	2.8 ± 0.7	1 ± 0	n/a	1.4 ± 0.3
Axon & Bifurcations Total Length (μm)	165.4 ± 44.8	76.2 ± 38.7	n/a	79.3 ± 24.6

Note. Data are mean ± SE for number of cells in parentheses. A one-way ANOVA was used to compare each firing type against the other for each of the morphological properties. A Tukey HSD *post-hoc* test was used for multiple comparisons. Significantly different from LS (*, $p < .05$) and significantly different from ADP-RS (#, $p < .05$).

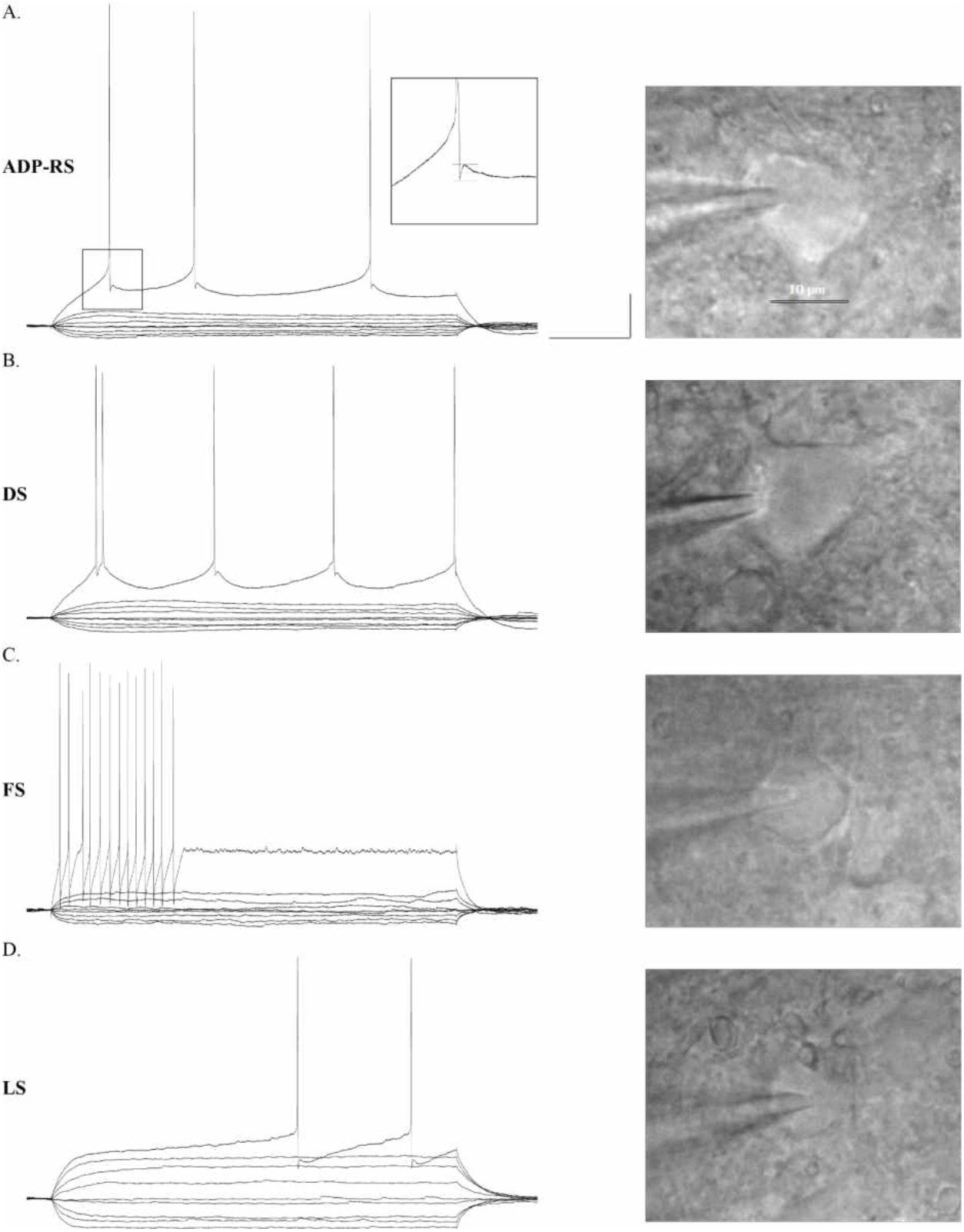

Figure 1. (A-D) Representative waveforms of GRS neurons demonstrating I-V relationships and a current injection ~20 pA above threshold to demonstrate typical firing pattern (scale bar 100 ms & 20 mV). On the right are representative DIC-images of neurons during recording. (A) afterderpolarizing regular-spiking (ADP-RS), (B) double-spiking (DS), (C) fast-spiking (FS), and (D) late-spiking (LS).

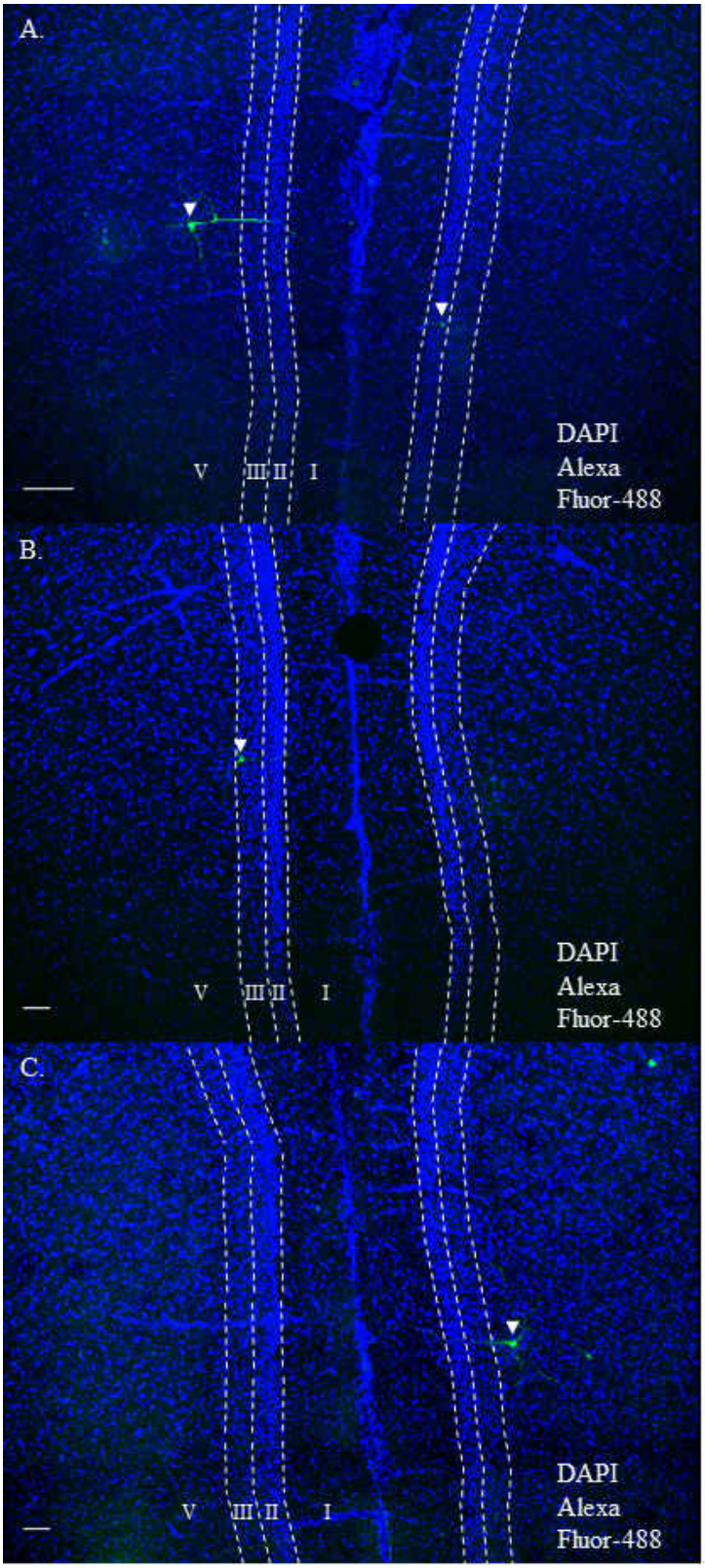

Figure 2. Representative dual channel dapi and alexa fluor-488 images used to determine the laminar location of recorded neurons. A) On the left a layer V neuron is indicated with an arrow head and on the right a layer II neuron. B) A layer III neuron is indicated with an arrow head. C) A layer V neuron is indicated with an arrow head. Scale bars 50 µm.

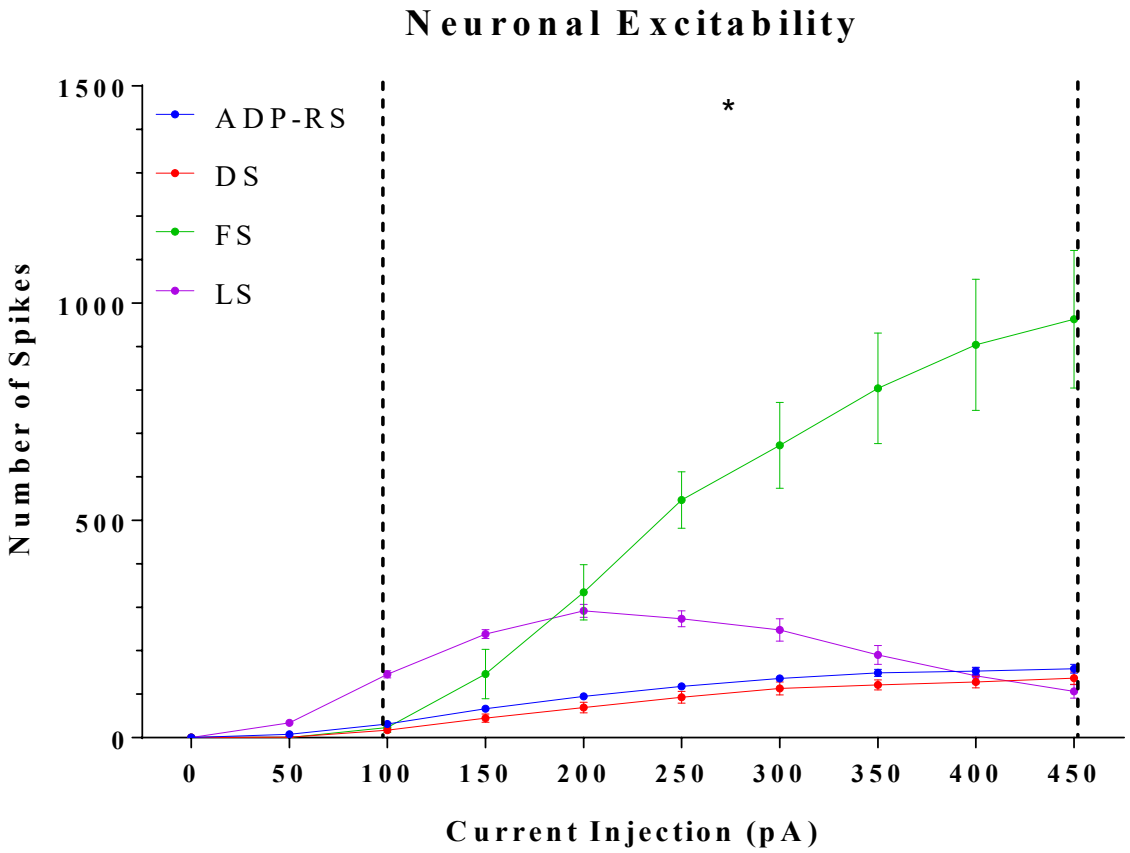

Figure 3. Mean number of spikes in response to ascending current injections analyzed by firing type. A two way ANOVA on neuronal excitability revealed a main effect of firing type ($F_{(3, 1138)} = 537.8$, $p < .01$), current injection ($F_{(9, 1138)} = 137.4$, $p < .01$), and an interaction effect ($F_{(27, 1138)} = 57.81$, $p < .01$). *Post-hoc* analysis revealed that there are statistically significant differences between firing types in the number of AP's fired from 100-450 pA injected: at 100 pA – ADP-RS, DS, FS < LS ($p < .01$ for all comparisons), at 150 pA – ADP-RS, DS < LS ($p < .01$ for all comparisons), at 200 pA – ADP-RS, DS < LS; ADP-RS, DS < FS ($p < .01$ for all comparisons), at 250 pA – ADP-RS, DS < LS; ADP-RS, DS, LS < FS ($p < .01$ for all comparisons), at 300 pA – ADP-RS, DS < LS; ADP-RS, DS, LS < FS ($p < .01$ for all comparisons), at 350 pA –ADP-RS, DS, LS < FS ($p < .01$ for all comparisons), at 400 pA – ADP-RS, DS, LS < FS ($p < .01$ for all comparisons), at 450 pA –ADP-RS, DS, LS < FS; ADP-RS > LS ($p < .01$ for all comparisons).

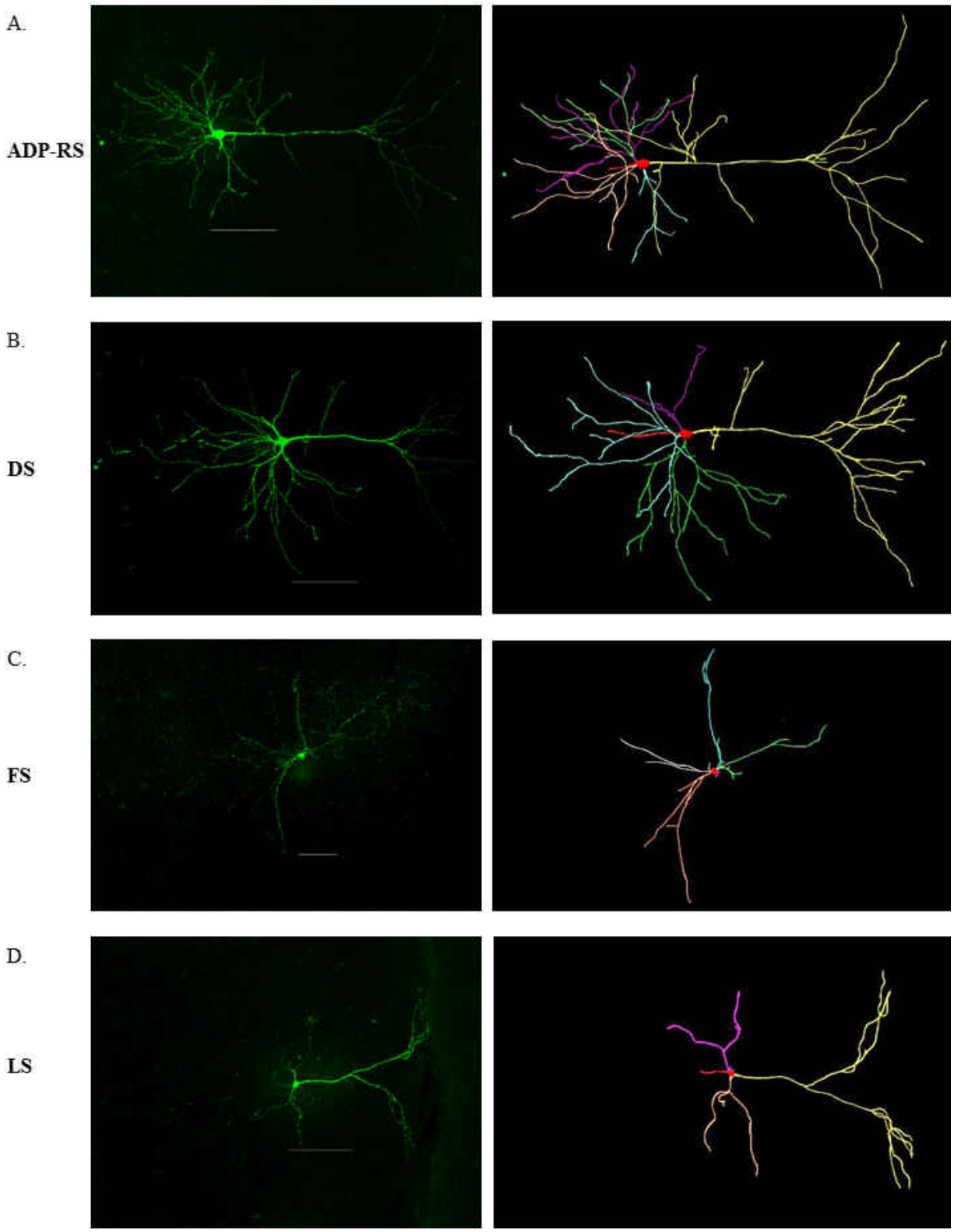

Figure 4. Representative Z-stack projections of GRS neurons on the left and their reconstructions on the right. The neuron shown in image C required a stack-stitch imaging protocol to capture the entire extent of its dendrites. Scale bars 100 µm.

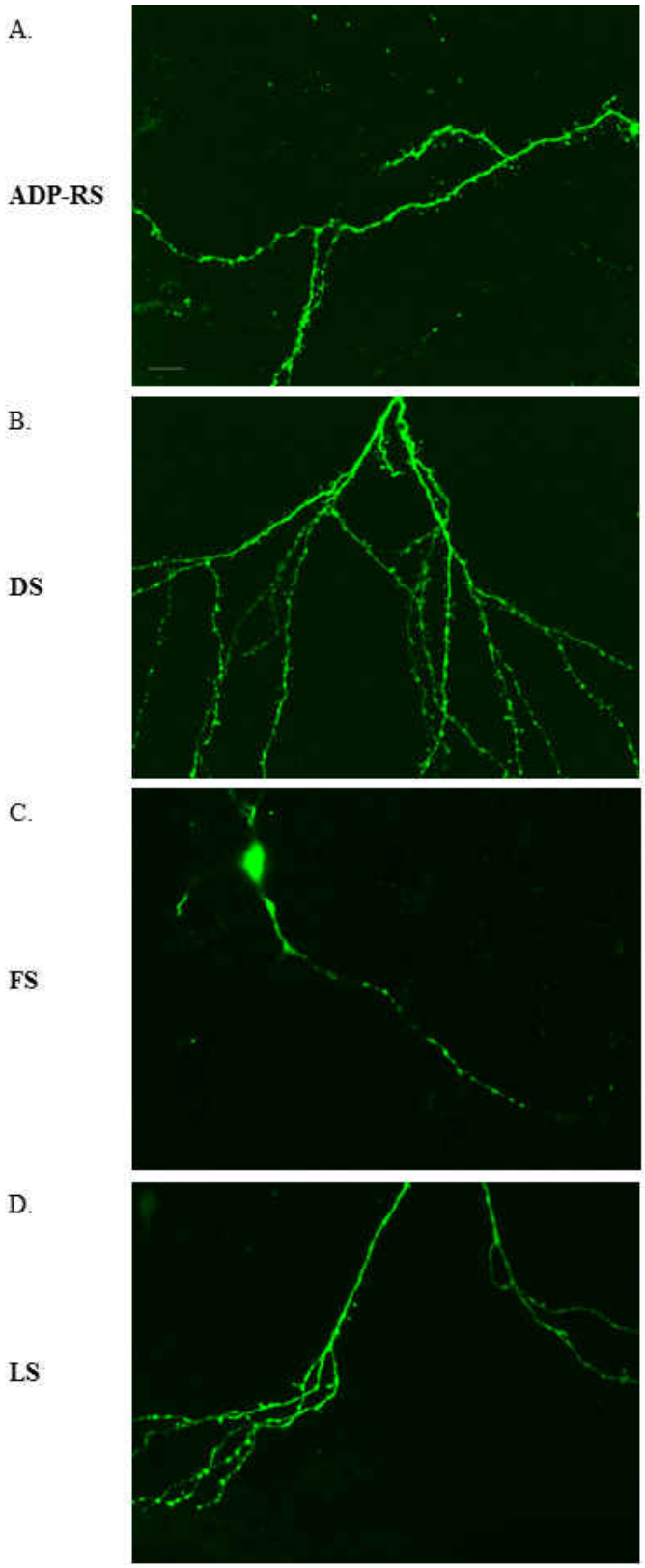

Figure 5. Representative Z-stack projections of GRS neuron spines, visualized at 100X (scale 10 µm). The majority of ADP-RS, DS and LS neurons had distinguishable spines on both the apical and basilar dendrites, but no FS neurons had any distinguishable spines.

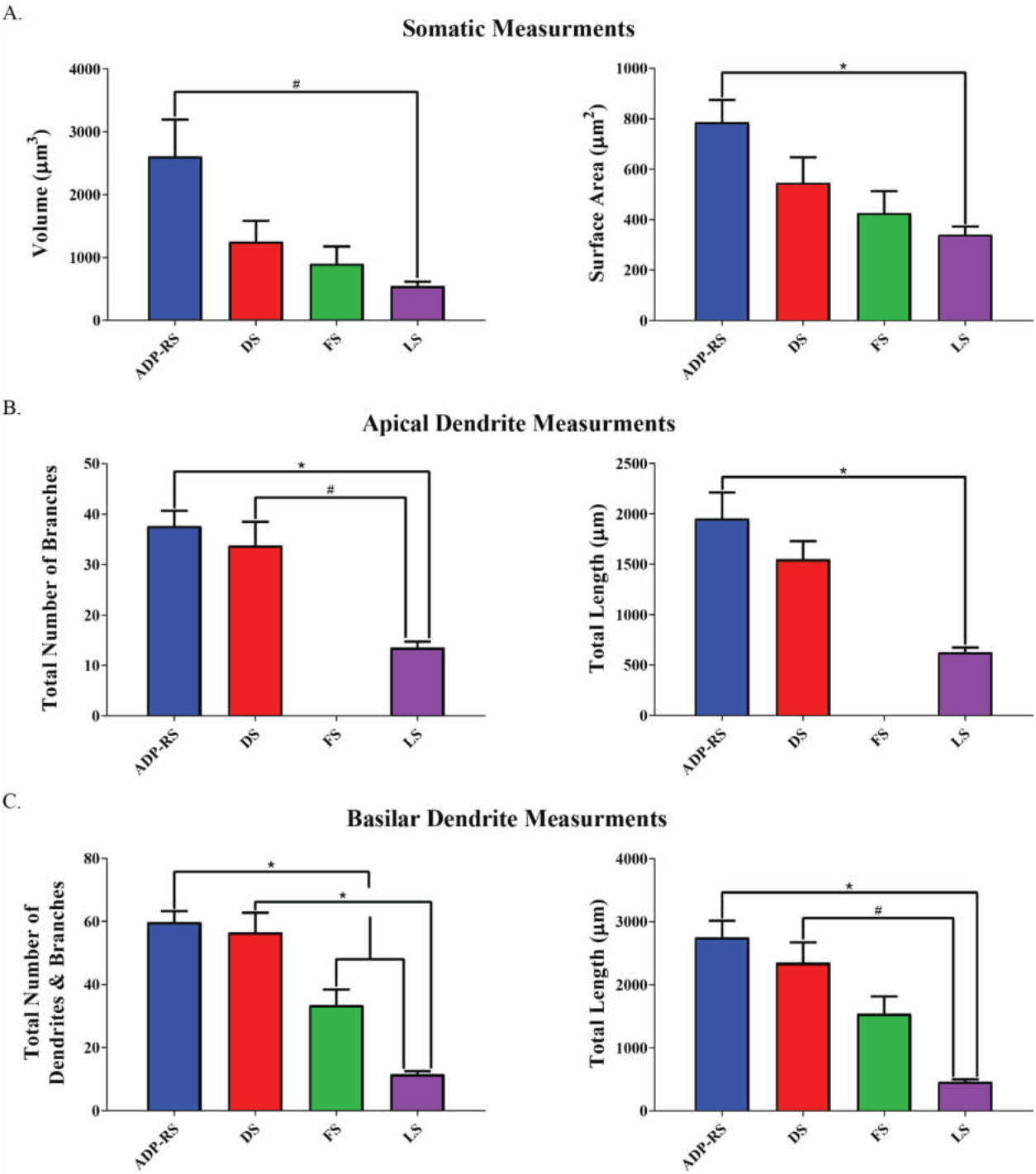

Figure 6. A one-way ANOVA revealed statistically significant main effects of firing type on soma surface area ($F_{(3, 70)} = 4.52$, $p < .01$), total number of apical dendrite branches ($F_{(2, 66)} = 14.85$, $p < .01$), total length of the apical dendrite and its branches ($F_{(2, 66)} = 6.38$, $p < .01$), total number of basilar dendrites and branches ($F_{(3, 70)} = 32.18$, $p < .01$), and total length of basilar dendrites and branches ($F_{(3, 70)} = 12.91$, $p < .01$). *Post-hoc* analysis revealed several differences: soma surface area - ADP-RS > LS neurons ($p < .01$); total number of apical dendrite branches - ADP-RS > LS neurons ($p < .01$); total length of apical dendrite and branches - ADP-RS > LS neurons ($p < .01$); total number of basilar dendrites and branches - ADP-RS > FS & LS neurons ($p < .01$) and DS > LS neurons ($p < .01$); and total length of basilar dendrites and branches - ADP-RS > LS neurons ($p < .01$).

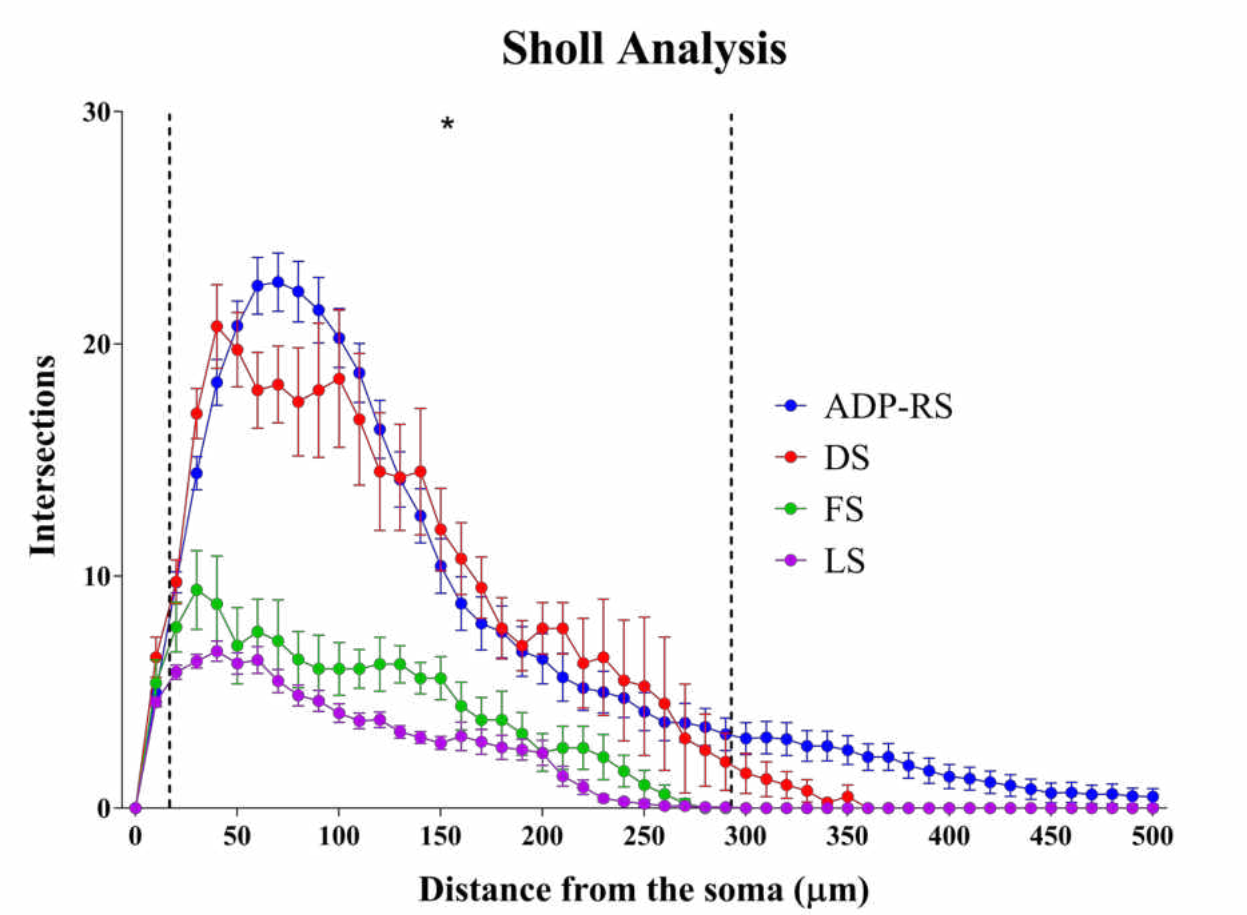

Figure 7. Dashed lines show the range of distances from the soma in which there are statistically significant differences between firing types, 20-290 µm. A two-way ANOVA revealed a statistically significant effect of distance from the soma ($F_{(50, 3570)} = 33.19$, $p < .01$), firing type ($F_{(3, 3570)} = 134.79$, $p < .01$), and an interaction effect ($F_{(150, 3570)} = 2.91$, $p < .01$). *Post-hoc* analysis revealed that there are significant differences in number of intersections between firing types from 20-290 µm from the soma; at 20 µm – ADP-RS > LS neurons ($p < .01$), at 30 µm – ADP-RS & DS > LS neurons ($p < .01$), from 40 µm to 140 µm ADP-RS & DS > FS & LS neurons ($p < .05$ for all comparisons), from 150 µm to 170 µm ADP-RS and DS > LS neurons ($p < .05$ for all comparisons), from 180 µm to 290 µm ADP-RS > LS neurons ($p < .05$ for all comparisons).

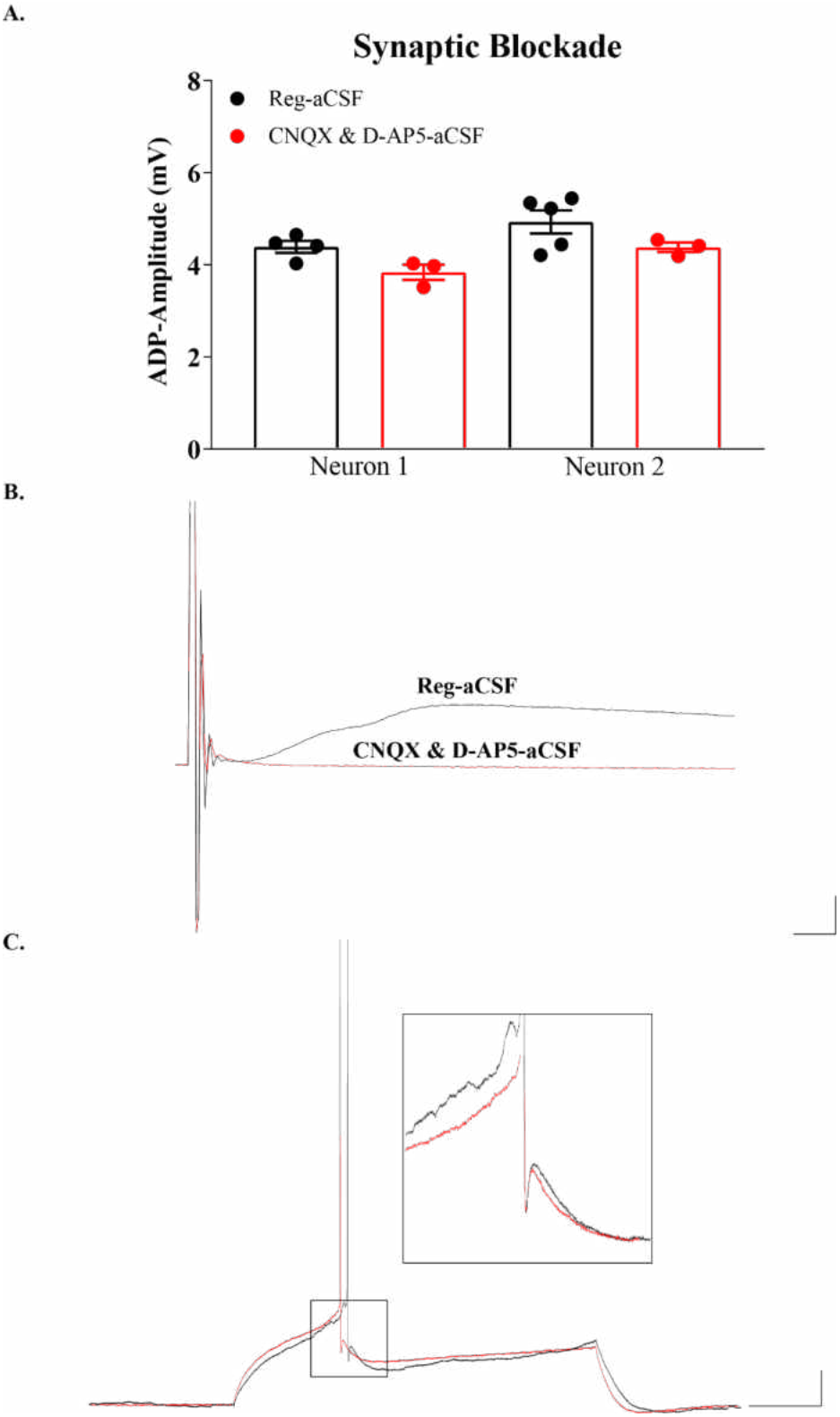

Figure 8. (A) A one-way ANOVA revealed a statistically significant main effect of aCSF on ADP-amplitude ($F_{(3, 11)} = 4.98$, $p < .05$). However, *post-hoc* analysis didn't find any significant differences within each experiment. (B) Sample waveforms illustrating the effect of CNQX & D-AP5 on an electrically evoked post-synaptic potential (scale bar 1 s & 10 mV). (C) Sample waveforms demonstrating the effect of CNQX & D-AP5 on ADP-amplitude (scale bar 100 ms & 10 mV).

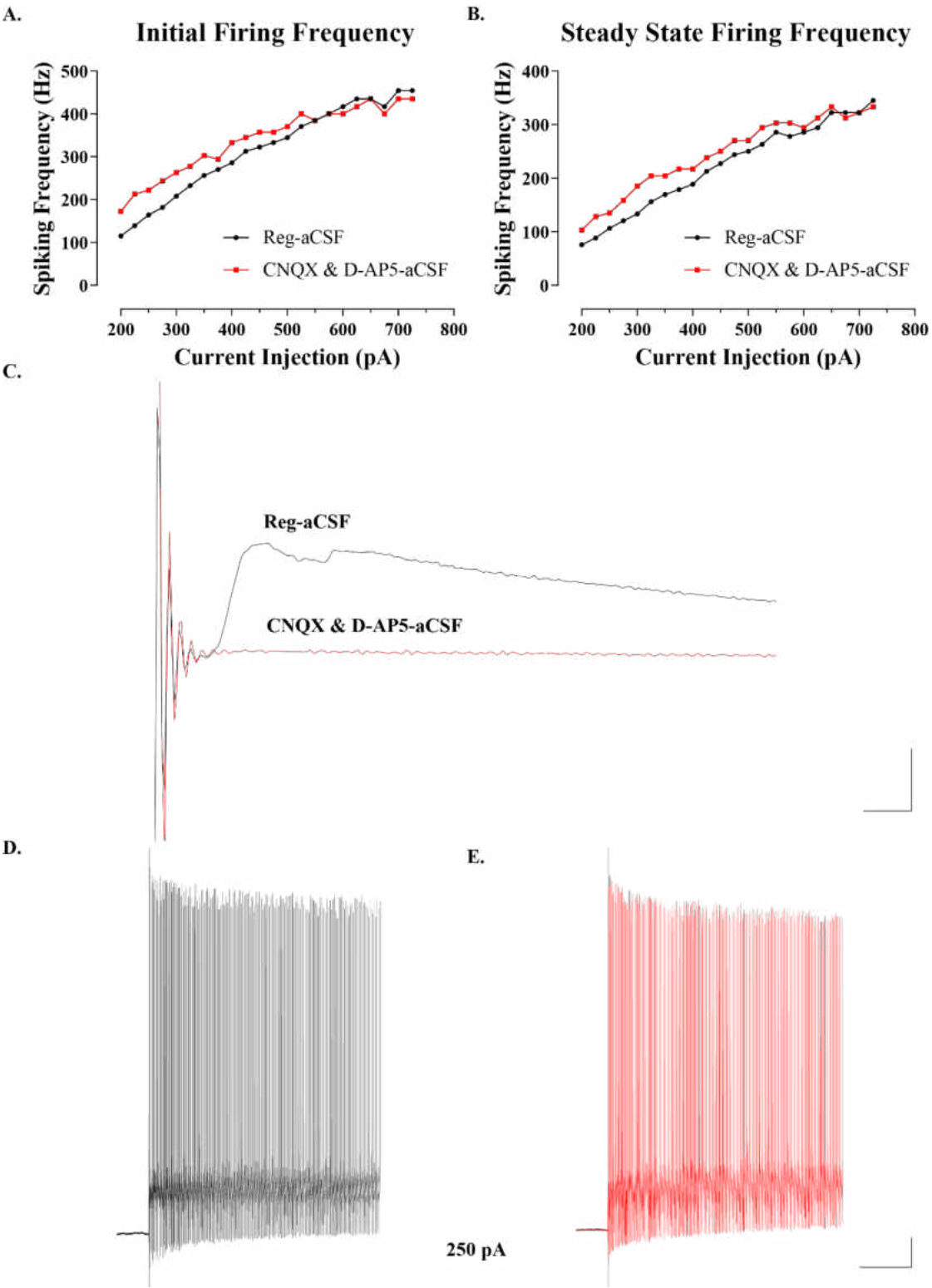

Figure 9. The bath application of CNQX (10 µm) & D-AP5 (30 µm) seemed to increase initial firing frequency at lower current injections (A) but the effect didn't persist. Similarly, CNQX & D-AP5 seemed to increase steady state firing initially (B) but the effect didn't seem to persist. However, the experiment has only been conducted in one FS cell, thus no statistical analysis was performed. (C) Sample waveforms illustrating the effect of CNQX & D-AP5 on an electrically evoked post-synaptic potential (scale bar 1 s & 10 mV). (D-E) First 2.5 s of sample waveforms demonstrating the effect of CNQX & D-AP5 on firing frequency (scale bar 500 ms & 10 mV).

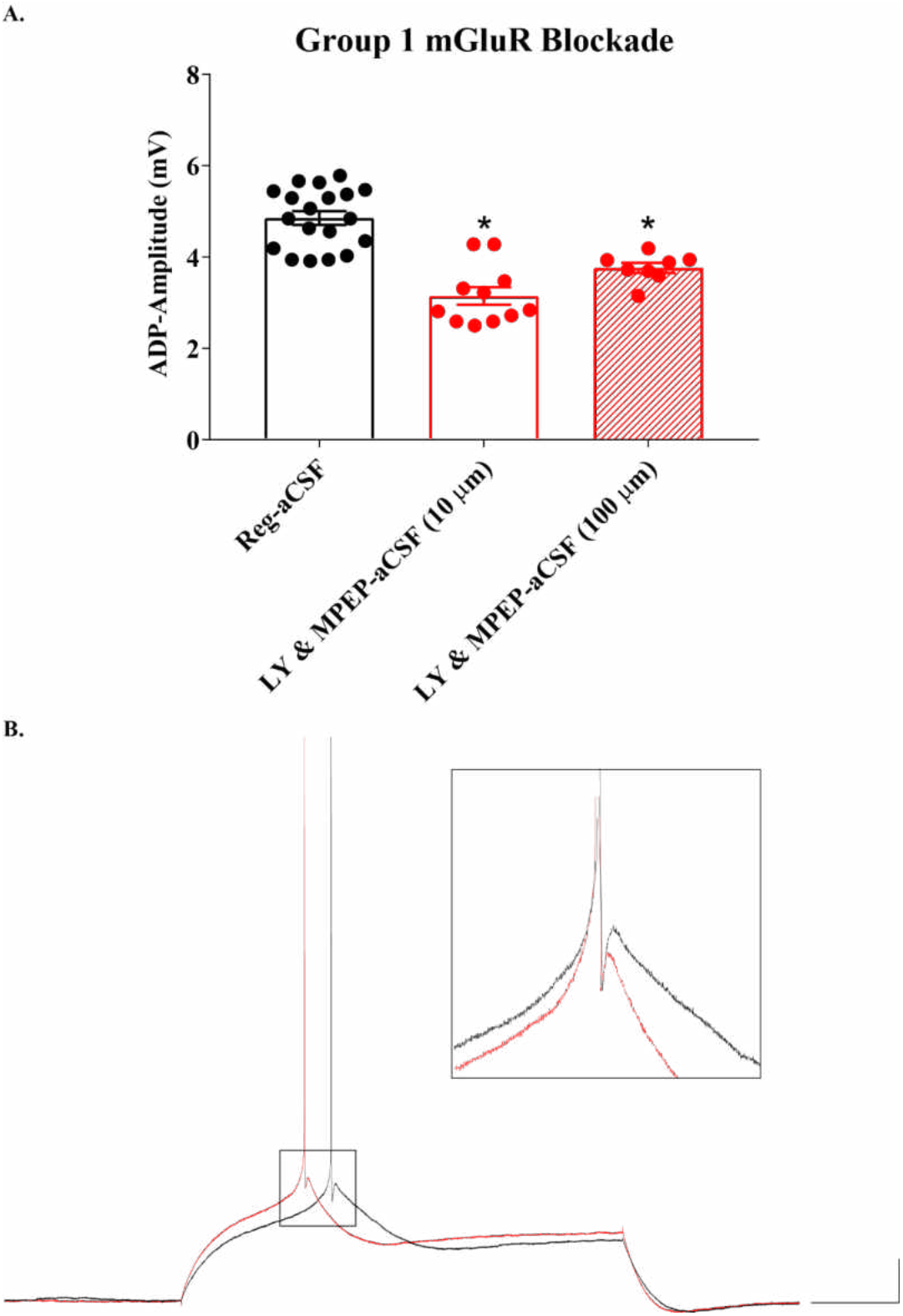

Figure 10. (A) A one-way ANOVA revealed a statistically significant main effect of aCSF on ADP-amplitude ($F_{(2, 35)} = 30.61$, $p < .01$). *Post-hoc* analysis revealed that bath application of LY367385 & MPEP at two concentrations, 10 µm and 100 µm, significantly reduced ADP-amplitude at both concentrations ($p < .01$ both comparisons) but the concentrations didn't significantly differ in their effect ($p = .1$). (B) Sample waveforms demonstrating the effect of LY367385 & MPEP on ADP-amplitude (scale bar 100 ms & 10 mV).

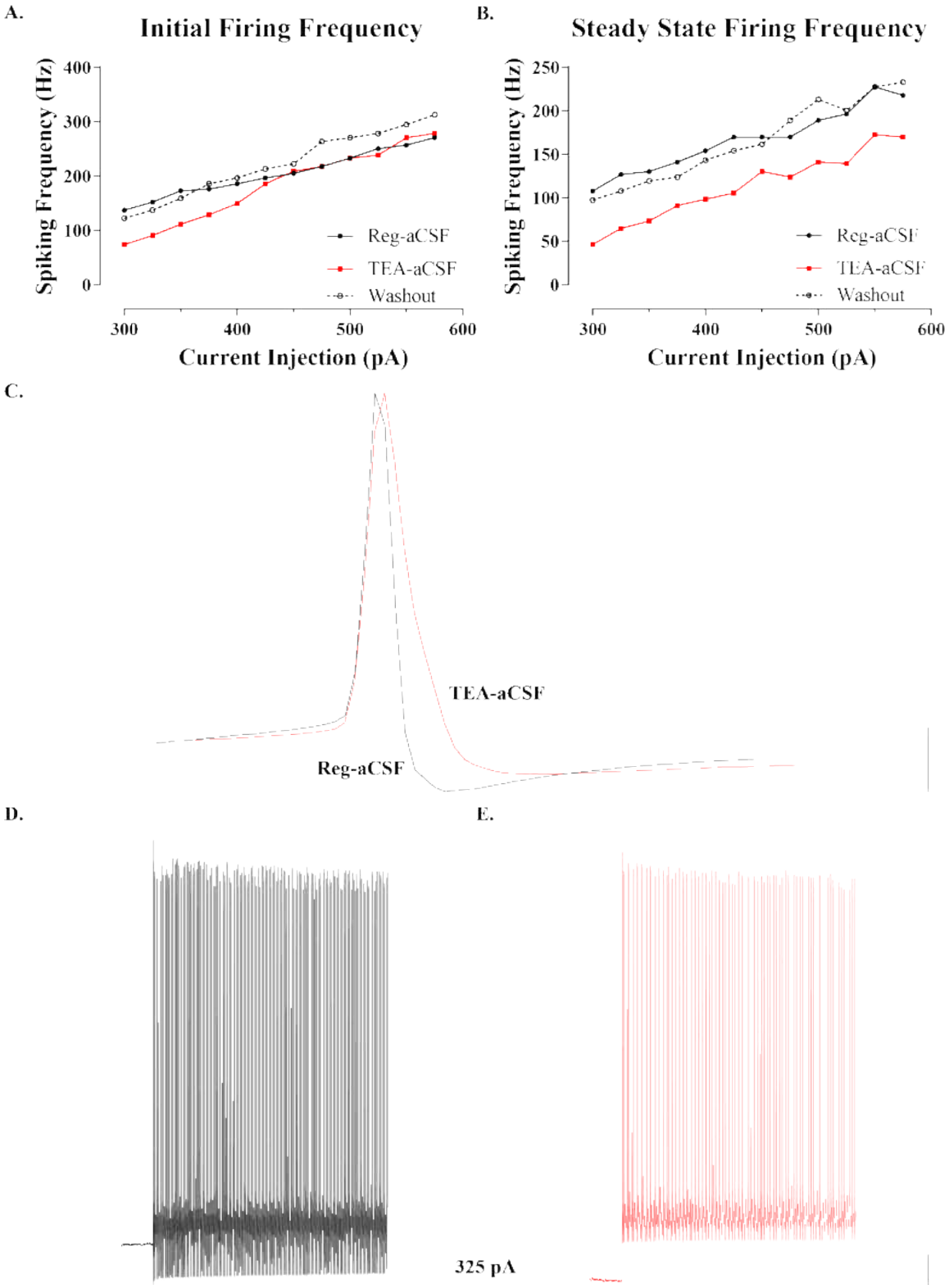

Figure 11. The bath application of TEA (1 mm) seemed to decrease initial firing frequency at lower current injections (A) but the effect didn't persist. Although, TEA did seem to persistently decrease steady state firing (B). However, the experiment has only been conducted in one cell, thus no statistical analysis was performed. (C) Sample waveforms illustrating the effect of TEA on the width of an AP (scale bar .5 ms & 20 mV). (D-E) First 2.5 s of sample waveforms demonstrating the effect of TEA on firing frequency (scale bar 500 ms & 10 mV).

References

Aggleton, J. P., Wright, N. F., and Vann, S. D., Saunders, R. C. (2012). Medial Temporal Lobe Projections to the Retrosplenial cortex of the Macaque Monkey. *Hippocampus,* 22, 1883-1900.

Aggleton, J. P., Saunders, R. C., Wright, N. F., and Vann, S. D. (2014). The origin of projections from the posterior cingulate and retrosplenial cortices to the anterior, medial dorsal and laterodorsal thalamic nuclei of macaque monkeys. *European Journal of Neuroscience,* 39, 107-123.

Alzheimer's Association. (2017). Alzheimer's Disease Facts and Figures. *Alzheimer's & Dementia*, 11(3), 332+.

Andrews-Hanna, J. R., Snyder, A. Z., Vincent, J. L., Lustig, C., Head, D., Raichle, M. E., and Buckner, R. L. (2007). Disruption of Large-Scale Brain Systems in Advanced Aging. *Neuron,* 56(5), 924-935.

Anglada-Figueroa, D., and Quirk, G. J. (2005). Lesions of the Basal Amygdala Block Expression of Conditioned Fear But Not Extinction. *The Journal of Neuroscience*, 25(42), 9680 9685.

Auger, S. D., Mullally, S. L., and Maguire, E. A. (2012). Retrosplenial Cortex Codes for Permanent Landmarks. *Plos One,* 7(8), 1-13.

Beck, H., and Yaari, Y. (2008). Plasticity of intrinsic neuronal properties in CNS disorders. *Nature Reviews Neuroscience,* 9(5), 357 – 369. Doi: 10.1038/nrn2371

Berger, T. W., Weikar, C. L., Bassett, J. L., and Orr, W. B. (1986). Lesions of the Retrosplenial Cortex Produce Deficits in Reversal Learning of the Rabbit Nictitating Membrane Response: Implications for Potential Interactions Between Hippocampal and Cerebellar Brain Systems. *Behavioral Neuroscience,* 100(6), 802-809.

Bishop, N. A., Lu, T., and Yanker, B. A. (2010). Neural mechanisms of aging and cognitive decline. *Nature,* 464, 529-535.

Blanchard, R. J., Blanchard, D. C. (1969). Crouching as an index of fear. *J Comp Physiol Psychol,* 67, 370 – 375.

Burgos-Robles, A., Vidal-Gonzalez, I., Santini, E., and Quirk, G. J. (2007). Consolidation of Fear Extinction Requires NMDA Receptor-Dependent Bursting in the Ventromedial Prefrontal Cortex. *Neuron,* 53, 871-880.

Burgos-Robles, A., Vidal-Gonzalez, I., and Quirk, G. J. (2009). Sustained Conditioned Responses in Prelimbic Prefrontal Neurons Are Correlated with Fear Expression and Extinction Failure. *The Journal of Neuroscience,* 29(26), 8474-8482.

Burwell, R. D., and Amaral, D. G. (1998). Perirhinal and Postrhinal Cortices of the Rat: Interconnectivity and Connections With the Entorhinal Cortex. *The Journal of Comparative Neurology,* 391, 293-321.

Cain, D. P., Humpartzoomian, R., and Boon, F. (2006). Retrosplenial cortex lesions impair water maze strategies learning or spatial place learning depending on propr experience of the rat. *Behavioural Brain Research,* 170, 316-325.

Cauli, B., Audinat, E., Lambolez, B., Angulo, M. C., Ropert, N., Tsuzuki, K . . . Rossier, J. (1997). Molecular and physiological diversity of cortical nonpyramidal cells. *The Journal of Neuroscience : The Official Journal of the Society for Neuroscience, 17*(10), 3894-906.

Chang, C., and Maren, S. (2011). Medial prefrontal cortex activation facilitates re-extinction of fear in rats. *Learning & Memory,* 18, 221-225.

Chen, L., Lin, L., Barnes, L., and McNaughton, C. (1994). Head-direction cells in the rat posterior cortex. *Experimental Brain Research, 101*(1), 24-34.

Cho, J., and Sharp, P. (2001). Head Direction, Place, and Movement Correlates for Cells in the Rat Retrosplenial Cortex. *Behavioral Neuroscience, 115*(1), 3-25.

Cohen-Matsliah, S., Rosenblum, K., and Barkai, E. (2009). Olfactory-learning abilities are correlated with the rate by which intrinsic neuronal excitability is modulated in the piriform cortex. *European Journal of Neuroscience,* 30(7), 1339-1348.

Cooper, B. G., and Mizumori, S. J. Y. (2001). Temporary Inactivation of the Retrosplenial Cortex Causes a Transient Reorganization of Spatial Coding in the Hippocampus. *The Journal of Neuroscience,* 21(11), 3966-4001.

Corcoran, K. A., Donnan, M. D., Tronson, N. C., Guzman, Y. F., Gao, C., Jovasevic, V., Guedea, A. L., and Radulovic, J. (2011). NMDA Receptors in Retrosplenial Cortex are Necessary for Retrieval of Recent and Remote Context Fear Memory. *The Journal of Neuroscience,* 31(32), 11655-11659.

Corcoran, K. A., Leaderbrand, K., and Radulovic, J. (2013). Extinction of Remotely Acquired Fear Depends on an Inhibitory NR2B/PKA Pathway in the Retrosplenial Cortex. *The Journal of Neuroscience,* 33(50), 19492-19498.

Czajkowski, R., Sugar, J., Zhang, S., Couey, J. J., Ye, J., and Witter, M. P. (2013). Superficially Projecting Principal Neurons in Layer V of Medial Entorhinal Cortex in the Rat Receive Excitatory Retrosplenial Input. *The Journal of Neuroscience,* 33(40), 15779-15792.

Daoudal, G., and Debanne, D. (2003). Long-term plasticity of intrinsic excitability: Learning rules and mechanisms. *Learning & Memory,* 10(6), 456-65.

Detert, J. A., Kampa, N. D., and Moyer, J. R. Jr. (2008). Differential Effects of Training Intertrial Interval on Acquisition of Trace and Long-Delay Fear Conditioning in Rats. *Behavioral Neuroscience,* 122(6), 1318 – 1327.

Dong, H., and Ennis, M. (2014). Activation of group I metabotropic glutamate receptors enhances persistent sodium current and rhythmic bursting in main olfactory bulb external tufted cells. *Journal of Neurophysiology,* 111(3), 641-7.

Erisir, A., Lau, D., Rudy, B., and Leonard, C. (1999). Function of specific K^+ channels in sustained high-frequency firing of fast-spiking neocortical interneurons. *Journal of Neurophysiology,* 82(5), 2476-89.

Fabbri, R., Furini, C., Passani, M., Provensi, G., Baldi, E., Bucherelli, C., . . . Blandina, P. (2016). Memory retrieval of inhibitory avoidance requires histamine H-1 receptor activation in the hippocampus. *Proceedings Of The National Academy Of Sciences Of The United States Of Ame,* 113(19), E2714-E2720.

Faulkner, B., & Brown, T. (1999). Morphology and physiology of neurons in the rat perirhinal-lateral amygdala area. *The Journal of Comparative Neurology, 411*(4), 613-42.

Foster, B., Kaveh, A., Dastjerdi, M., Miller, K., and Parvizi, J. (2013). Human retrosplenial cortex displays transient theta phase locking with medial temporal cortex prior to activation during autobiographical memory retrieval. *The Journal of Neuroscience,* 33(25), 10439-46.

Fowler, M. A., Sidiropoulou, K., Ozkan, E. D., Phillips, C. W., and Cooper, D. C. (2007). Corticolimbic Expression of TRPC4 and TRPC5 Channels in the Rodent Brain. *PLoS ONE*, *2*(6), e573. http://doi.org/10.1371/journal.pone.0000573

Freund, T., and Buzsaki, G. (1996). Interneurons of the hippocampus. *Hippocampus, 6*(4), 347-470.

Frick, A., Johnston, D., Spruston, N., and Cline, H. (2005). Plasticity of dendritic excitability. *Journal of Neurobiology,* 64(1), 100-115.

Funahashi, S. (2017). Working Memory in the Prefrontal Cortex. *Brain Sci,* 7(5), 49; doi: 10.3390/brainsci7050049

Gale, G. D., Anagnostaras, S. G., Godsil, B. P., Mitchell, S., Nozawa, T., Sage, J. R., Wiltgen, B., and Fanselow, M. S. (2004). Role of the Basolateral Amygdala in the Storage of Fear Memories across the Adult Lifetime of Rats. *The Journal of Neuroscience,* 24(15), 3810 3815.

Garden, D., Massey, P., Caruana, D., Johnson, B., Warburton, E., Aggleton, J., and Bashir, Z. (2009). Anterior thalamic lesions stop synaptic plasticity in retrosplenial cortex slices: Expanding the pathology of diencephalic amnesia. *Brain,* 132(7), 1847-1857.

Gilmartin, M. R., and Helmstetter, F. J. (2010). Trace and contextual fear conditioning require neural activity and NMDA receptor-dependent transmission in the medial prefrontal cortex. *Learning & Memory,* 17, 289-296.

Greene, C. C., Schwindt, P. C., and Crill, W. E. (1994). Properties and ionic mechanisms of a metabotropic glutamate receptor-mediated slow afterdepolarization in neocortical neurons. *Journal of Neurophysiology,* 72(2), 693 – 704.

Haider, B., Duque, A., Hasenstaub, A., and Mccormick, D. (2006). Neocortical network activity in vivo is generated through a dynamic balance of excitation and inhibition. *The Journal of Neuroscience: The Official Journal of the Society for Neuroscience, 26*(17), 4535-45.

Haj-Dahmane, S., and Andrade, R. (1997). Calcium-activated cation nonselective current contributes to the fast afterdepolarization in rat prefrontal cortex neurons. *Journal of Neurophysiology,* 78(4), 1983-9.

Haijima, A., and Ichitani, Y. (2012). Dissociable Anterograde Amnesic Effects of Retrosplenial Cortex and Hippocampal Lesions on Spontaneous Object Recognition Memory in Rats. *Hippocampus,* 22, 1868-1875.

Harland, B. C., Collings, D. A., McNaughton, N., Abraham, W. C., and Dalrymple-Alford J. C. (2014). Anterior Thalamic Lesions Reduce Spine Density in Both Hippocampal CA1 and Retrosplenial Cortex, but Enrichment Rescues CA1 Spines Only. *Hippocampus*, 24, 1232-1247.

Helmstetter, F. J. (1992). Contribution of the Amygdala to Learning and Performance of Conditional Fear. *Physiology & Behavior,* 51, 1271-1276.

Helmstetter, F. J., and Bellgowan, P. S. (1994). Effects of Muscimol Applied to the Basolateral Amygdala on Acquisition and Expression of Contextual Fear Conditioning in Rats. *Behavioral Neuroscience,* 108(5), 1005-1009.

Hindley, E. L., Nelson, A. J. D., Aggleton, J. P., and Vann, S. D. (2014). Dysgranular retrosplenial cortex lesions in rats disrupt cross-modal object recognition. *Learning & Memory,* 21, 171-179.

Hofmann, M. E., and Frazier, C. J. (2010). Muscarinic receptor activation modulates the excitability of hilar mossy cells through the induction of an afterdepolarization. *Brain Research,* 1318, 42-51.

Houser, C., Hendry, R., Jones, S., and Vaughn, H. (1983). Morphological diversity of immunocytochemically identified GABA neurons in the monkey sensory-motor cortex. *Journal of Neurocytology, 12*(4), 617-638.

Ichinohe, N., Knight, A., Ogawa, M., Ohshima, T., Mikoshiba, K., Yoshihara, Y., Terashima, T.,

and Rockland K. S. (2008). Unusual Patch–Matrix Organization in the Retrosplenial Cortex of the reeler Mouse and Shaking Rat Kawasaki. *Cereb Cortex*, 18 (5): 1125-1138. doi: 10.1093/cercor/bhm148

Insel, N., and Barnes, C. (2015). Differential Activation of Fast-Spiking and Regular-Firing Neuron Populations During Movement and Reward in the Dorsal Medial Frontal Cortex. *Cerebral Cortex, 25*(9), 2631-2647.

Ireland, D., and Abraham, W. (2002). Group I mGluRs increase excitability of hippocampal CA1 pyramidal neurons by a PLC-independent mechanism. *Journal of Neurophysiology, 88*(1), 107-16.

Jacob, P., Casali, G., Spieser, L., Page, H., Overington, D., and Jeffery, K. (2017). An independent, landmark-dominated head-direction signal in dysgranular retrosplenial cortex. *Nature Neuroscience,* 20(2), 173-175.

Jenkins, T. A., Vann, S. D., Amin, E., and Aggleton, J. P. (2004). Anterior thalamic lesions stop immediate early gene activation in selective laminae of the retrosplenial cortex: evidence of covert pathology in rats?. *European Journal of Neuroscience,* 19, 3291-3304.

Jones, E. (1993). GABAergic neurons and their role in cortical plasticity in primates. *Cerebral Cortex (New York, N.Y.: 1991), 3*(5), 361-72.

Kaczorowski, C. C., and Disterhoft, J. F. (2009). Memory Deficits Are Associated with Impaired Ability to Modulate Neuronal Excitability in Middle-Aged Mice. *Learning & Memory,* 16(6), 362-366.

Kaczorowski, C. C., Davis, S. J., and Moyer, J. R. Jr. (2012). Aging redistributes medial prefrontal neuronal excitability and impedes extinction of trace fear conditioning. *Neurobiology of Aging,* 33(8), 1744-1757.

Kawaguchi, Y. (1995). Physiological subgroups of nonpyramidal cells with specific morphological characteristics in layer II/III of rat frontal cortex. *J. Neurosci,* 15: 2638–2655.

Kawaguchi, Y., and Kubota, Y. (1997). GABAergic cell subtypes and their synaptic connections in rat frontal cortex. *Cerebral Cortex, 7*(6), 476-486.

Keene, C. S., and Bucci, D. S. (2008a). Neurotoxic Lesions of Retrosplenial Cortex Disrupt Signaled and Unsignaled Contextual Fear Conditioning. *Behavioral Neuroscience,* 122(5). 1070-1077.

Keene, C. S., and Bucci, D. S. (2008b). Contributions of the Retrosplenial and Posterior Parietal Cortices to Cue-Specific and Contextual Fear Conditioning. *Behavioral Neuroscience,* 122(1), 89-97.

Keene, C. S., and Bucci, D. S. (2008c). Involvement of the Retrosplenial Cortex in Processing

Multiple Conditioned Stimuli. *Behavioral Neuroscience*, 122(3), 651-658.

Keene, C. S., and Bucci, D. S. (2009). Damage to the retrosplenial cortex produces specific impairments in spatial working memory. *Neurobiology of Learning and Memory,* 91, 408-414.

Kobayashi, Y., and Amaral, D. G. (2003). Macaque Monkey Retrosplenial Cortex: II. Cortical Efferents. *The Journal of Comparative Neurology,* 466, 48 – 79.

Kobayashi, Y., and Amaral, D. G. (2007). Macaque Monkey Retrosplenial Cortex: III. Cortical Efferents. *The Journal of Comparative Neurology,* 502, 810 – 833.

Kurotani, T., Miyashita, T., Wintzer, M., Konishi, T., Sakai, K., Ichinohe, N., and Rockland, K. S. (2013). Pyramidal neurons in the superficial layers of rat retrosplenial cortex exhibit a late-spiking firing property. *Brain Struct Funct,* 218, 239-254.

Kwapis, J. L., Jarome, T. J., Lee, J. L., and Helmstetter, F. J. (2015). The retrosplenial cortex is involved in the formation of memory for context and trace fear conditioning. *Neurobiology of Learning and Memory,* 123, 110 – 116.

Kwapis, J. L., Jarome, T. J., Lee, J. L., Gilmartin, M. R., and Helmstetter, F. J. (2014). Extinguishing trace fear engages the retrosplenial cortex rather than the amygdala. *Neurobiology of Learning and Memory,* 113, 41-54.

Lei, Y., Thuault, S. J., Launay, P., Margolskee, R. F., Kandel, E. R., and Siegelbaum, S. A. (2014). Differential contribution of TRPM4 and TRPM5 nonselective cation channels to the slow afterdepolarization in mouse prefrontal cortex neurons. *Frontiers in Cellular Neuroscience,* 8(NA), NA.

Logue, S. F., Paylor, R., and Wehner, J. M. (1997). Hippocampal Lesions Cause Learning Deficits in Inbred Mice in the Morris Water Maze and Conditioned-Fear Task. *Behavioral Neuroscience.* 111(1), 104-113.

Maren, S., Aharonov, G., and Fanselow, M. S. (1996). Retrograde Abolition of Conditional Fear After Excitotoxic Lesions in the Basolateral Amygdala of Rats: Absence of a Temporal Gradient. *Behavioral Neuroscience,* 10(4), 718-726.

Martina, M., Royer, S., & Paré, D. (1999). Physiological properties of central medial and central lateral amygdala neurons. *Journal of Neurophysiology, 82*(4), 1843-54.

Matsuo, R., and Kang, Y. (1998). Two types of parasympathetic preganglionic neurones in the superior salivatory nucleus characterized electrophysiologically in slice preparations of neonatal rats. *Journal of Physiology, 513*(1), 157-170.

McEchron, M. D., Bouwmeester, H., Tseng, W., Weiss, C., and Disterhoft, J. F. (1998). Hippocampectomy Disrupts Auditory Trace Fear Conditioning and Contextual Fear

Conditioning in the Rat. *Hippocampus,* 8, 638-646

McEchron, M. D., Tseng, W., and Disterhoft, J. F., (2000). Neurotoxic Lesions of the Dorsal Hippocampus Disrupt Auditory-Cued Trace Heart Rate (Fear) Conditioning in Rabbits. *Hippocampus,* 10, 739-751.

McEchron, M. D., Cheng, A. Y., and Gilmartin, M. R. (2004). Trace fear conditioning is reduced in the aging rat. *Neurobiology of Learning and Memory,* 82, 71-76.

Mckay, B., Matthews, E., Oliveira, F., and Disterhoft, J. (2009). Intrinsic neuronal excitability is reversibly altered by a single experience in fear conditioning. *Journal of Neurophysiology,* 102(5), 2763-70.

Misane, I., Tovote, P., Meyer, M., Spiess, J., Ogren, S. O., and Stiedl, O. (2005). Time Dependent Involvement of the Dorsal Hippocampus in Trace fear Conditioning in Mice. *Hippocampus,* 15, 418-426.

Miyashita, T., and Rockland, K. S. (2007). GABAergic projections from the hippocampus to the retrosplenial cortex in the rat. *European Journal of Neuroscience,* 26, 1193-1204.

Monyer, H., Jonas, P. (2009). Polymerase Chain Reaction Analysis of Ion Channel Expression in Single Neurons of Brain Slices. In Sakmann, B., Neher, E., (Eds.), *Single-Channel Recording* (pp. 357-373). Doi:10.1007/978-1-4419-1229-9_16

Morris, R., Pandya, D., and Petrides, M. (1999). Fiber system linking the mid-dorsolateral frontal cortex with the retrosplenial/presubicular region in the rhesus monkey. *The Journal of Comparative Neurology,* 407 (2), 183-92.

Motanis, H., Maroun, M., and Barkai, E. (2014). Learning-Induced Bidirectional Plasticity of Intrinsic Neuronal Excitability Reflects the Valence of the Outcome. *Cerebral Cortex,* 24(4), 1075-1087.

Moyer, J. R. Jr., Deyo, R. A., and Disterhoft, J. F. (1990). Hippocampectomy Disrupts Trace Eye Blink Conditioning in Rabbits. *Behavioral Neuroscience*, 104(2), 243-252.

Moyer, J. R. Jr., Thompson, L. T., & Disterhoft, J. F. (1996). Trace eyeblink conditioning increases CA1 excitability in a transient and learning-specific manner. *Journal of Neuroscience,* 16(17), 5536 – 5546.

Moyer, J. R. Jr., McNay, E. C., and Brown, T. H. (2002). Three Classes of Pyramidal Neurons in Layer V of Rat Perirhinal Cortex. *Hippocampus,* 12, 218-234.

Moyer, J. R. Jr., and Brown, T. H. (2006). Impaired Trace and Contextual Fear Conditioning in Aged Rats. *Behavioral Neuroscience*, 120(3), 612-624.

Moyer, J. R. Jr., Brown, T. H. (2007). Visually-guided patch-clamp recordings in brain slices. In:

Advanced techniques for patch-clamp analysis, Ed 2 (Walz W, ed), pp 169 – 227. Totowa, NJ: Humana.

Murakami, K., Ishikawa, Y., and Sato, F. (2013). Localization of α7 nicotinic acetylcholine receptor immunoreactivity on GABAergic interneurons in layers I–III of the rat retrosplenial granular cortex. *Neuroscience,* 252, 443-459.

Nikoletopoulou, V., and Tavernarakis, N. (2012). Calcium homeostasis in aging neurons. *Frontiers in Genetics,* 3(200) 1-17.

Nisenbaum, E., Xu, Z., and Wilson, C. (1994). Contribution of a slowly inactivating potassium current to the transition to firing of neostriatal spiny projection neurons. *Journal of Neurophysiology, 71*(3), 1174-89.

Nisenbaum, E., and Wilson, C. (1995). Potassium currents responsible for inward and outward rectification in rat neostriatal spiny projection neurons. *The Journal of Neuroscience: The Official Journal of the Society for Neuroscience, 15*(6), 4449-63.

Nishimura, Y., Asahi, M., Saitoh, K., Kitagawa, H., Kumazawa, Y., Itoh, K., . . . Yamamoto, T. (2001). Ionic mechanisms underlying burst firing of layer III sensorimotor cortical neurons of the cat: An in vitro slice study. *Journal of Neurophysiology,* 86(2), 771-81.

Nixima, K., Okanoya, K., and Kurotani, T. (2013). Current source-density analysis of intracortical circuit in the granular retrosplenial cortex of rats: A possible role in stimulus time buffering. *Neuroscience Research, 76*(1-2), 52-57.

Oda, S., Funato, H., Sato, F., Adachi-Akahane, S., Ito, M., Takase, K., Kuroda, M. (2014). A Subset of Tahalamocortical Projections to the Retrosplenial Cortex Possesses Two Vesicular Glutamate Transporter Isoforms, VGluT1 and VGluT2, in Axon Terminals and Somata. *The Journal of Comparative Neurology,* 522, 2089-2106.

Oh, M. M., Kuo, A. G., Wu, W. W., Sametsky, E. A., and Disterhoft, J. F. (2003). Watermaze learning enhances excitability of CA1 pyramidal neurons. *Journal Of Neurophysiology,* 90(4), 2171-2179.

Oh, M. M., Oliveira, F. A., and Disterhoft, J. F. (2010). Learning and aging related changes in intrinsic neuronal excitability. *Frontiers in Aging Neuroscience,* 2(1), 1-10.

Okada, T., Shimizu, S., Wakamori, M., Maeda, A., Kurosaki, T., Takada, N., . . . Mori, Y. (1998). Molecular cloning and functional characterization of a novel receptor-activated TRP Ca2+ channel from mouse brain. *The Journal of Biological Chemistry,* 273(17), 10279-87.

Olney, J. W., Labruyere, J., and Price, M. T. (1989). Pathological Changes Induced in Cerebrocortical Neurons by Phencyclidine and Related Drugs. *Science,* 244(4910), 1360-1362.

Ortman, J. M., Velkoff, V. A., and Hogan, H. (2014). An Aging Nation: The Older Population in the United States. *U.S. Census Bureau.*

Papoutsi, A., Sidiropoulou, K., Cutsuridis, V., and Poirazi, P. (2013). Induction and modulation of persistent activity in a layer V PFC microcircuit model. *Frontiers In Neural Circuits, 7*, Frontiers In Neural Circuits, 2013 Oct 9, Vol.7.

Park, J., Remy, S., Varela, J., Cooper, D., Chung, S., Kang, H., . . . Bacci, A. (2010). A Post-Burst Afterdepolarization Is Mediated by Group I Metabotropic Glutamate Receptor-Dependent Upregulation of Ca v 2.3 R-Type Calcium Channels in CA1 Pyramidal Neurons (mGluR Activation Produces a Post-Burst ADP). *PLoS Biology,* 8(11), E1000534.

Paxinos, G., Watson, C. (2007). *The Rat Brain in Stereotaxic Coordinates*. Burlington, MA: Elsevier Inc.

Pengas, G. Hodges, J. R., Watson, P., and Nestor, P. J. (2010). Focal posterior cingulate atrophy in incipient Alzheimer's disease. *Neurobiology of Aging,* 25-33.

Philipp, S., Trost, C., Warnat, J., Rautmann, J., Himmerkus, N., Schroth, G., . . . Flockerzi, V. (2000). TRP4 (CCE1) protein is part of native calcium release-activated Ca2+-like channels in adrenal cells. *Journal Of Biological Chemistry,* 275(31), 23965-23972.

Pothuizen, H, H.J., Davies, M., Aggleton, J. P., Vann, S. D. (2010). Effects of selective granular retrosplenial cortex lesions on spatial working memory in rats. *Behavioural Brain Research,* 208, 566 – 575.

Prasad, J. A., and Chudasama, Y. (2013). Viral Tracing Identifies Parallel Disynaptic Pathways to the Hippocampus. *The Journal of Neuroscience,* 33(19), 8494-8503.

Quinn, J. J., Ma, Q. D., Tinsley, M. R., Koch, C., and Fanselow, M. S. (2008). Inverse temporal contributions of the dorsal hippocampus and medial prefrontal cortex to the expression of long-term fear memories. *Learning & Memory,* 15, 368-372.

Redish, D. A., and Touretzky, D. S. (1998). The Role of the Hippocampus in Solving the Morris Water Maze. *Neural Computation,* 10, 73-111.

Ribak, C. (1978). Aspinous and sparsely-spinous stellate neurons in the visual cortex of rats contain glutamic acid decarboxylase. *Journal of Neurocytology,7*(4), 461-478.

Robinson, S., Poorman, C. E., Marder, T. J., and Bucci, D. J. (2012). Identification of Functional Circuitry between Retrosplenial and Postrhinal Cortices during Fear Conditioning. *The Journal of Neuroscience,* 32(35), 12076-12086.

Rudy, B., Chow, A., Lau, D., Amarillo, Y., Ozaita, A., Saganich, M., . . . Vega-Saenz de Miera, E.

(1999). Contributions of Kv3 channels to neuronal excitability. *Annals of the New York Academy of Sciences,* 868, 304-43.

Runyan, J. D., Moore, A. N., and Dash, P. K. (2004). A Role for Prefrontal Cortex in Memory Storage for Trace Fear Conditioning. *The Journal of Neuroscience,* 24(6), 1288-1295.

Saar, D., Grossman, Y., and Barkai, E. (1998). Reduced after-hyperpolarization in rat piriform cortex pyramidal neurons is associated with increased learning capability during operant conditioning. *European Journal of Neuroscience,* 10(4), 1518-1523.

Salaj, M., Druga, R., Cerman, J., Kubová, H., and Barinka, F. (2015). Calretinin and parvalbumin immunoreactive interneurons in the retrosplenial cortex of the rat brain: Qualitative and quantitative analyses. *Brain Research,* 1627, 201-215.

Sanchez-Vives, M. V., and Mccormick, D. A. (2000). Cellular and network mechanisms of rhythmic recurrent activity in neocortex. *Nature Neuroscience, 3*(10), 1027-34.

Santini, E., Quirk, G., and Porter, J. (2008). Fear conditioning and extinction differentially modify the intrinsic excitability of infralimbic neurons. *The Journal of Neuroscience,* 28(15), 4028-36.

Santini, E., and Porter, J. (2010). M-type potassium channels modulate the intrinsic excitability of infralimbic neurons and regulate fear expression and extinction. *The Journal of Neuroscience,* 30(37), 12379-86.

Sehgal, M., Song, C., Ehlers, V., and Moyer, J. R. Jr. (2013). Learning to learn – Intrinsic plasticity as a metaplasticity mechanism for memory formation. *Neurobiology of Learning and Memory,* 105, 186-199.

Sehgal, M., Ehlers, V. L., and Moyer, J. R. Jr. (2014). Learning Enhances Intrinsic Excitability in a Subset of Lateral Amygdala Neurons.*Learning & Memory,* 21(3), 161-170.

Seltzer, B., Pandya, D. N. (2009). Posterior cingulate and retrosplenial cortex connections of the caudal superior temporal region in the rhesus monkey. *Exp Brain Res,* 195, 325-334.

Shibata, Kondo, and Naito. (2004). Organization of retrosplenial cortical projections to the anterior cingulate, motor, and prefrontal cortices in the rat. *Neuroscience Research,* 49(1), 1-11.

Shibata, H., and Naito, J. (2008). Organization of Anterior Cingulate and Frontal Cortical Projections to the Retrosplenial Cortex in the Rat. *The Journal of Comparative Neurology,* 506, 30-45.

Shibata, H., Honda, Y., Sasaki, H., and Naito, J. (2009). Organization of intrinsic connections of the retrosplenial cortex in the rat. *Anat Sci Int,* 84, 280-292.

Shu, Y., Hasenstaub, A., and Mccormick, D. A. (2003). Turning on and off recurrent balanced cortical activity. *Nature,423*(6937), 288-93.

Sidiropoulou, K., Lu, F., Fowler, M. A., Xiao, R., Phillips, C., Ozkan, E. D. . . . Cooper, D. C. (2009). Dopamine modulates an mGluR5-mediated depolarization underlying prefrontal persistent activity. *Nature Neuroscience, 12*(2), 190-199.

Sidiropoulou, K., and Poirazi, P. (2012). Predictive Features of Persistent Activity Emergence in Regular Spiking and Intrinsic Bursting Model Neurons (Predictive Features of Persistent Activity). *PLoS Computational Biology, 8*(4), E1002489.

Sigwald, E. L., Genoud, M. E., Giachero, M., de Olmos, S., Molina, V. A., and Lorenzo, A. (2015). Selective neuronal degeneration in the retrosplenial cortex impairs the recall of contextual fear memory. *Brain Struct Funct, DOI 10.1007/s00429-015-1008-9.*

Song, C., Detert, J., Sehgal, M., and Moyer, J. R. Jr. (2012). Trace fear conditioning enhances synaptic and intrinsic plasticity in rat hippocampus. *Journal of Neurophysiology,* 107(12), 3397-408.

Song, C., Ehlers, V. L., Moyer, J. R. Jr. (2015). Trace Fear Conditioning Differentially Modulates Intrinsic Excitability of Medial Prefrontal Cortex-Basolateral Complex of Amygdala Projection Neurons in Infralimbic and Prelimbic Cortices. *The Journal of Neuroscience,* 35(39), 13524-13511.

Storm, J. (1988). Temporal integration by a slowly inactivating K+ current in hippocampal neurons. *Nature, 336*(6197), 379.

Sugar, J., Witter, M. P., van Strien, N. M., Cappaert. N. L. M. (2011). The retrosplenial cortex: intrinsic connectivity and connections with the (para) hippocampal region in the rat. An interactive connectome. *Frontiers in Neuroinformatics, doi: 10.3389/fninf.2011.00007*.

Tanaka, K. Z., Pevzner, A., Hamidi, A. B., Nakazawa, Y., Graham, J., and Wiltgen, B. J. (2014). Cortical Representations Are Reinstated by the Hippocampus during Memory Retrieval. *Neuron,* 84(2), 347-354.

Thomson, L. T., Moyer, J. R. Jr., & Disterhoft, J. F. (1996). Transient changes in excitability of rabbit CA3 neurons with a time course appropriate to support memory consolidation. *Journal of Neurophysiology,* 76(3), 1836 – 1849.

Thomson, A. M., West, D. C., Hahn, J., and Deuchars, J. (1996). Single axon IPSPs elicited in pyramidal cells by three classes of interneurones in slices of rat neocortex. *Journal Of Physiology-London, 496*(1), 81-102.

Todd, T. P., and Bucci, D. J. (2015). Retrosplenial Cortex and Long-Term Memory: Molecules to Behavior. *Neural Plasticity,* 1-9.

Van Groen, T., and Wyss, J. M. (1990). Connections of the retrosplenial granular a cortex in the rat. *The Journal of Comparative Neurology,* 300(4), 593-606.

Van Groen, T., and Wyss, J. M. (1992). Connections of the retrosplenial dysgranular cortex in the rat. *The Journal of Comparative Neurology,* 315(2), 200-216.

Van Groen, T., and Wyss, J. M. (2003). Connections of the retrosplenial granular b cortex in the rat. *The Journal of Comparative Neurology,* 463, 249-263.

Vann, S. D., Aggleton, J. P., and Maguire, E. A. (2009). What does the retrosplenial cortex do?. *Nature Reviews,* 10, 792-802.

Vann, S. D., and Aggleton, J. P. (2005). Selective Dysgranular Retrosplenial Cortex Lesions in Rats Disrupt Allocentric Performance of the Radial-Arm Maze Task. *Behavioral Neuroscience,* 119(6), 1682-1686.

Varela, J., Wang, J., Christianson, J., Maier, S., and Cooper, D. (2012). Control over stress, but not stress per se increases prefrontal cortical pyramidal neuron excitability. *The Journal of Neuroscience,* 32(37), 12848-53.

Vedder, L., Miller, A., Harrison, M., and Smith, D. (2016). Retrosplenial Cortical Neurons Encode Navigational Cues, Trajectories and Reward Locations During Goal Directed Navigation. *Cerebral Cortex,* 1-11.

Vidal-Gonzalez, I., Vidal-Gonzalez, B., Rauch, S. L., and Quirk, G. J. (2006). Microstimulation reveals opposing influences of prelimbic and infralimbic cortex on the expression of conditioned fear. *Learning & Memory,* 13, 728-733.

Villain, N., Desgranges, B., Viader, F., Sayette, V., Mezenge, F., Landeau, B., Baron, J. C., Eustache, F., and Chetelat, G. (2008). Relationships between Hippocampal Atrophy, White Matter Disruption, and Gray Matter Hypometabolism in Alzheimer's Disease. *The Journal of Neuroscience,* 28(24), 6174-6181.

Villarreal, J. S., Dykes, J. R., and Barea-Rodriguez, E. J. (2004). Fischer 344 Rats Display Age Related Memory Deficits in Trace Fear Conditioning. *Behavioral Neuroscience*, *118*(6), 1166-1175.

Vogt, B. A., and Miller, M. W. (1983). Cortical connections between rat cingulate cortex and visual, motor, and postsubicular cortices. *The Journal of Comparative Neurology,* 216(2), 192-210.

Washburn, M., and Moises, H. (1992). Electrophysiological and morphological properties of rat basolateral amygdaloid neurons in vitro. *The Journal of Neuroscience: The Official Journal of the Society for Neuroscience, 12*(10), 4066-79.

Whissell, P., Cajanding, J., Fogel, N., & Kim, J. C. (2015). Comparative density of CCK- and

PV-GABA cells within the cortex and hippocampus. *Frontiers in Neuroanatomy, 9*(124). doi:10.3389/fnana.2015.00124

Wilber, A. A., Clark, B. J., Demecha, A. J., Mesina, L., Vos, J. M., and McNaughton, B. L. (2015). Cortical connectivity maps reveal anatomically distinct areas in the parietal cortex of the rat. *Frontiers in Neural Circuits,* 8(146), 1-15.

Wu, R., and Barish, M. (1999). Modulation of a slowly inactivating potassium current, I-D, by metabotropic glutamate receptor activation in cultured hippocampal pyramidal neurons. *Journal of Neuroscience, 19*(16), 6825-6837.

Wyss. M. J., Van Groen, T., and Sripanidkulchai, K. (1990). Dendritic Bundling in Layer I of Granular Retrosplenial Cortex: Intracellular Labeling and Selectivity of Innervation. *The Journal of Comparative Neurology.* 295, 33-42.

Yamawaki, N., Radulovic, J., and Shepherd, G. M. G. (2016) A Corticocortical Circuit Directly Links Retrosplenial Cortex to M2 in the Mouse. *The Journal of Neuroscience,* 36(36), 9365-9374.

Yan, H., Villalobos, C., and Andrade, R. (2009). TRPC Channels Mediate a Muscarinic Receptor-Induced Afterdepolarization in Cerebral Cortex. *The Journal of Neuroscience,* 29(32), 10038-46.

Zhang, W., and Linden, D. J. (2003). The other side of the engram: Experience-driven changes in neuronal intrinsic excitability. *Nature Reviews Neuroscience,* 4(11), 885.